1. Experiment as a Boundary-Value Problem

A fluid flow experiment is an attempt to isolate a part of the world and measure flow and thermodynamic properties. A fluid is defined as a material that deforms continuously if a shear stress is applied. An internal flow situation has walls bounding the flow, but an inflow and outflow position must be controlled. An external flow problem has a uniform flow far from the body of interest. In both situations the state of flow at the boundary is controlled. In the mathematical representation of the flow, the flow conditions on the boundary are specified. This is the nature of the governing physics. If the boundary conditions depend on time the flow situation in the entire region must be specified at the initial time.

In what follows the major physical laws are outlined. In most cases tensor calculus in symbolic form is employed. Scalars are lightface type, vectors are boldface type, and tensors are boldface capitals. However, in cases where confusion is possible with tensor multiplications, index notation is employed. Scalars are then without an index, vectors have one index and tensors have two or more indices.

1.1 Thermodynamic Equations

The properties of a continuum are defined by an imaginary experiment where a region of volume V with characteristic length L is imagined to contain molecules. At a given position the volume is reduced around that position as indicated by the limit process $L \to 0$. A typical molecule, denoted by the subscript i, has a mass m_i and an instantaneous velocity $\boldsymbol{v}_i$. The density is the sum of mass over all molecules in the region divided by the volume as the limit is taken. Although $L \to 0$ is indicated, it cannot become so small that fluctuations occur because only a few molecules are present.

$$\rho = \lim_{L \to 0} \frac{\sum m_i}{V} \,. \tag{1.1}$$

The mass-averaged velocity is a vector average of the molecular velocities and mass. This is appropriate to

measure the momentum:

$$\boldsymbol{v} = \lim_{L\to 0} \frac{\sum m_i \boldsymbol{v}_i}{\sum m_i} \,. \tag{1.2}$$

If the substance has several chemical species, $n^{(k)}$ moles in the region, a molar averaged velocity for each species k is

$$V^{(k)} = \lim_{L\to 0} \frac{\sum \boldsymbol{v}_i^{(k)}}{n^{(k)}} \,. \tag{1.3}$$

Such a velocity is useful in diffusion problems. The internal energy (per unit mass) due to random translational motions of the molecules is

$$e = \lim_{L\to 0} \frac{\sum \frac{1}{2} m_i (\boldsymbol{v}_i - \boldsymbol{v}) \cdot (\boldsymbol{v}_i - \boldsymbol{v})}{\sum m_i} \,. \tag{1.4}$$

The total internal energy includes other molecular motions such as vibrations, and configuration energies. The properties above are well defined whether or not the substance is in thermodynamic equilibrium.

1.1.1 Thermodynamics

It is assumed that the bulk motion of the substance does not affect the thermodynamic state. All thermodynamic variables of a simple compressible substance are described by a fundamental law that gives the entropy $s = s(\rho, e)$ or in another form $e = e(s, \rho)$. Each substance has its own entropy function, however, all functions obey the fundamental differential equation of thermodynamics.

$$e = e(s, \rho) \tag{1.5}$$

$$\mathrm{d}e = T\,\mathrm{d}s - p\,\mathrm{d}(\rho^{-1}) \,, \tag{1.6}$$

the thermodynamic pressure is defined by

$$p(s, \rho) \equiv \left.\frac{\partial e}{\partial(\rho^{-1})}\right|_s \,, \tag{1.7}$$

and the temperature is given by

$$T(s, \rho) \equiv \left.\frac{\partial e}{\partial s}\right|_\rho \,. \tag{1.8}$$

Other thermodynamic properties follow from their definitions, for example the enthalpy $h = e + p/\rho$.

Two equations of state are equivalent to the fundamental law of a substance. The first equation of state is of the form

$$p = p(\rho, T) \tag{1.9}$$

or

$$\rho = \rho(p, T) \,. \tag{1.10}$$

It is equivalent to specify the compressibility coefficient functions:

$$\alpha(p, T) \equiv \left.\frac{1}{\rho}\frac{\partial \rho}{\partial p}\right|_T \,, \tag{1.11}$$

$$\beta(p, T) \equiv -\left.\frac{1}{\rho}\frac{\partial \rho}{\partial T}\right|_p \,. \tag{1.12}$$

Integration of these functions will reproduce $\rho = \rho(p, T)$.

The second equation of state is that for energy:

$$e = e(\rho, T) \,. \tag{1.13}$$

The important derivative function here is the specific heat (per unit mass) at constant volume:

$$c_\mathrm{v}(\rho, T) \equiv \left.\frac{\partial e}{\partial T}\right|_\rho \,. \tag{1.14}$$

The other function $\partial e/\partial\rho|_T$ is related to the state equation $\rho = \rho(p, T)$ by thermodynamic theory. In summary, the functions $p = p(\rho, T)$ and $c_\mathrm{v} = c_\mathrm{v}(\rho, T)$ describe the thermodynamics of a substance.

Often the enthalpy $h = e + p/\rho$ is used in preference to the internal energy. The important derivative function here is the specific heat (per unit mass) at constant pressure:

$$c_\mathrm{p}(p, T) \equiv \left.\frac{\partial h}{\partial T}\right|_p \,. \tag{1.15}$$

The other function $\partial h/\partial p|_T$ is related to the state equation $\rho = \rho(p, T)$ by thermodynamic theory. Alternatively, the functions $p = p(\rho, T)$ and $c_\mathrm{p} = c_\mathrm{p}(p, T)$ describe the thermodynamics of a substance.

There are special approximations of importance: the perfect gas, ideal gas, and incompressible fluid. For a perfect gas the state equations are:

$$p = \rho R T \,, \tag{1.16}$$

$$e = c_\mathrm{v}(\rho, T) T \,. \tag{1.17}$$

Alternatively, $h = c_\mathrm{p}(\rho, T)T$. A further restriction to an ideal gas gives simpler forms,

$$e = c_\mathrm{v}(T) T \tag{1.18}$$

$$h = c_\mathrm{v}(T) T + p/\rho \tag{1.19}$$

$$c_\mathrm{p}(T) = c_\mathrm{v}(T) + R \tag{1.20}$$

where R is the specific gas constant.

An incompressible fluid has thermodynamic variables that are independent of the density. The fundamental equation is

$$s = s(e)\,, \tag{1.21}$$

$$\mathrm{d}e = T\,\mathrm{d}s\,. \tag{1.22}$$

As before, the temperature is defined by

$$T \equiv \left.\frac{\partial e}{\partial s}\right|_{\rho}\,. \tag{1.23}$$

Pressure is a mechanical variable that is independent of the thermodynamic state. The first equation of state does not exist, and the second equation of state is

$$e = e(T) = c_{\mathrm{v}}(T)T\,. \tag{1.24}$$

The enthalpy is a mixture of thermodynamic and mechanical properties, $h = e + p/\rho$.

1.2 Kinematic Equations

A fluid particle is an imaginary collection of fluid that locally follows the fluid velocity. Due to random molecular motions a fluid particle does not consist of the same molecules for all time. There are two mathematical viewpoints with different independent space and time variables. The dependent variables, the thermodynamic properties and characteristics of the continuum motion (velocity vorticity, strain rate, etc.) are instantaneous concepts and are the same from either viewpoint. The Lagrangian view can be thought of as a history of a certain fluid particle. Independent variables in the Lagrangian viewpoint are the initial position of the particle and the time, $\boldsymbol{x}^0$ and $\hat{t}$. The particle position vector $\boldsymbol{r}$ is

$$\boldsymbol{r} = \tilde{\boldsymbol{r}}(\boldsymbol{x}^0, \hat{t}\,)\,, \tag{1.25}$$

It follows from this that the particle velocity is

$$\boldsymbol{v} = \frac{\partial \tilde{\boldsymbol{r}}}{\partial \hat{t}}\,. \tag{1.26}$$

and that the particle acceleration is

$$\boldsymbol{a} = \frac{\partial \boldsymbol{v}}{\partial \hat{t}}\,. \tag{1.27}$$

Alternately, the Eulerian viewpoint is based on a fixed position in space and time. The independent variables are $\boldsymbol{x}$ and t. In this viewpoint the particle position is

$$\boldsymbol{r} = \boldsymbol{r}(\boldsymbol{x}, t) = \boldsymbol{x}\,. \tag{1.28}$$

Equating $\boldsymbol{r}$ and time provides the connection between the two viewpoints.

$$\boldsymbol{x} = \tilde{\boldsymbol{r}}(\boldsymbol{x}^0, \hat{t}\,)\,, \tag{1.29}$$

$$t = \hat{t}\,. \tag{1.30}$$

For a given particle $\boldsymbol{x}^0$, the particle path, with time as a parameter, is

$$\boldsymbol{x}_p = \tilde{\boldsymbol{r}}(\boldsymbol{x}^0, t)\,. \tag{1.31}$$

Choosing a different initial particle $\boldsymbol{x}^0$ gives a different particle path.

Next, consider a line of particles given by an equation $\boldsymbol{x}^0 = \boldsymbol{x}^0(a)$ where a is a parameter that varies over some range, say $0 \le a \le 1$, where $a = 0$ is the beginning of the line and $a = 1$ is the end of the line. For given time t, a streak line of particles originally at $\boldsymbol{x}^0$ are at

$$\boldsymbol{x}_{\mathrm{str}} = \tilde{\boldsymbol{r}}\big(\boldsymbol{x}^0(a), t\big)\,. \tag{1.32}$$

A line of marked particles would move through the flow according to (1.31).

Another important concept is that of a streamline. For given time t, a streamline is everywhere tangent to the velocity

$$\boldsymbol{v} \times \mathrm{d}\boldsymbol{x}_{\mathrm{stm}} = 0\,,$$

or

$$\frac{\mathrm{d}x}{u} = \frac{\mathrm{d}y}{v} = \frac{\mathrm{d}z}{w}\,. \tag{1.33}$$

The second version above refers to a coordinate system x, y, z with velocity components u, v, w.

Any dependent property f can be expressed in Eulerian variables $f = f_{\mathrm{E}}(\boldsymbol{x}, t)$ or in Lagrangian variables $f = f_{\mathrm{L}}(\boldsymbol{x}^0, \hat{t})$. A Lagrangian time rate of change, the rate of change following a fluid particle, is given by

$$\frac{\partial f_L}{\partial \hat{t}}\,. \tag{1.34}$$

The particle velocity and acceleration are

$$v_i = \frac{\partial \tilde{r}}{\partial \hat{t}} = \frac{\mathrm{d}x_i}{\mathrm{d}t}\,, \tag{1.35}$$

$$a_i = \frac{\partial v_i}{\partial \hat{t}}\,. \tag{1.36}$$

By using the chain rules of differentiation of a composite function one finds that the Eulerian representation

of a Lagrangian time derivative is

$$\frac{\partial f_{\mathrm{L}}}{\partial \hat{t}} = \frac{\partial f_{\mathrm{E}}}{\partial t} + \boldsymbol{v}\cdot\nabla f_{\mathrm{E}} \,. \tag{1.37}$$

The right-hand side is called the Stokes derivative, the substantial derivative, or the material derivative.

$$\frac{\mathrm{d}f_{\mathrm{E}}}{\mathrm{d}t} \equiv \frac{\partial f_{\mathrm{E}}}{\partial t} + \boldsymbol{v}_i \frac{\partial f_{\mathrm{E}}}{\partial x_i} \,.$$

This offers a physical interpretation for this combination of terms.

In addition to the translational velocity, every point in the fluid has a vorticity. Given a fluid particle P at x, the solid-like rotation of a near neighbor at P' is the angular velocity $\boldsymbol{\omega}(x)/2$. By definition

$$\boldsymbol{\omega} = \nabla \times \boldsymbol{v} \,. \tag{1.38}$$

The rate of strain at P is defined as

$$S_{ij} = \frac{1}{2}(\partial_i \boldsymbol{v}_j + \partial_j \boldsymbol{v}_i);\ \boldsymbol{S} = \frac{1}{2}\left[(\nabla \boldsymbol{v}) + (\nabla \boldsymbol{v})^T\right] . \tag{1.39}$$

Consider two particles P at x and a near neighbor at P' at a distance ds in direction of a unit vector $\boldsymbol{n}$ from P. The strain velocity per unit distance is the strain vector $\boldsymbol{d}$.

$$\frac{\mathrm{d}\boldsymbol{v}_{\mathrm{strain}}}{\mathrm{d}s} = \boldsymbol{d} = \boldsymbol{n}\cdot\boldsymbol{S} \,. \tag{1.40}$$

A small material region has a volumetric rate of expansion

$$\lim_{L\to 0} \frac{1}{V_{MR}} \frac{\mathrm{d}V_{\mathrm{MR}}}{\mathrm{d}t} = \nabla\cdot\boldsymbol{v} \,. \tag{1.41}$$

This is of course zero for an incompressible flow.

1.3 Balance Laws and Local Governing Equations

1.3.1 Continuity

The law for conservation of mass yields the *continuity* equation, referring to the fact that the underlying assumption of a continuum is required.

$$\frac{1}{\rho}\frac{\mathrm{d}\rho}{\mathrm{d}t} + \nabla\cdot\boldsymbol{v} = 0 \,. \tag{1.42}$$

The fractional rate of change of density following a fluid particle and the rate of expansion of the material region form a balance. Another viewpoint, from a fixed point in space, gives a balance of the local rate of change of density and the divergence of the flux of fluid into the point:

$$\frac{\partial \rho}{\partial t} + \nabla\cdot(\rho\boldsymbol{v}) = 0 \,. \tag{1.43}$$

The continuity equation is used to derive a relation between the substantial derivative of any fluid property f_{E} and the local and convective derivatives of f_{E} observed at a fixed Eulerian location.

$$\rho\left(\frac{\partial f_{\mathrm{E}}}{\partial t} + \boldsymbol{v}\cdot\nabla f_{\mathrm{E}}\right) = \frac{\partial\,(\rho f_{\mathrm{E}})}{\partial t} + \nabla\cdot(\rho\boldsymbol{v} f_{\mathrm{E}}) \,. \tag{1.44}$$

1.3.2 Linear Momentum and Related Equations

The linear momentum per unit mass, $\boldsymbol{v}$, responds to surface and volumetric forces. The surface stress $\boldsymbol{R}$ on an area with outward normal $\boldsymbol{n}$ is the force per unit area of the outside substance upon the inside substance. The variation of this stress with surface direction is given by $\boldsymbol{n}$ and the variation with location is given by a stress tensor $\boldsymbol{T}(\boldsymbol{x}, t)$:

$$\boldsymbol{R} = \boldsymbol{n}\cdot\boldsymbol{T} \,. \tag{1.45}$$

The stress is divided into a viscous tensor and pressure by subtracting the thermodynamic pressure.

$$\boldsymbol{T} = -p\boldsymbol{\delta} + \boldsymbol{\tau} \,. \tag{1.46}$$

The trace of the stress tensor forms a mechanical pressure force:

$$p_{\mathrm{m}} = -\frac{1}{3}\mathrm{tr}(\boldsymbol{T}) = -\frac{1}{3}\sum_i T_{ii} \,. \tag{1.47}$$

The Stokes assumption equates these pressures, $p = p_{\mathrm{m}}$.

The gravity force per unit volume is $\rho\boldsymbol{g}$ where $\boldsymbol{g}$ is a constant scalar magnitude g times a unit vector in the gravity direction. If Z is the height above a horizontal reference plane,

$$\boldsymbol{F}_{\mathrm{g}} = -\rho g \nabla Z \,. \tag{1.48}$$

Two equivalent forms of the momentum are from the perspective of a fixed point in space or from the

perspective of a material particle

$$\frac{\partial(\rho \boldsymbol{v})}{\partial t} + \nabla\cdot(\rho \boldsymbol{v}^2) = -\nabla p + \nabla\cdot\boldsymbol{\tau} + \rho \boldsymbol{g}\,,$$
$$\rho\frac{\mathrm{d}\boldsymbol{v}}{\mathrm{d}t} = -\nabla p + \nabla\cdot\boldsymbol{\tau} + \rho \boldsymbol{g}\,. \qquad (1.49)$$

An equation governing the mechanical energy or kinetic energy per unit mass is obtained by the dot product of velocity and the momentum equation.

$$\frac{\partial\left(\rho\frac{1}{2}\boldsymbol{v}^2\right)}{\partial t} + \nabla\cdot\left(\rho \boldsymbol{v}\frac{1}{2}\boldsymbol{v}^2\right)$$
$$= -\boldsymbol{v}\cdot\nabla p + \rho\, v\cdot\boldsymbol{g} + \boldsymbol{v}\cdot(\nabla\cdot\boldsymbol{\tau})\,. \qquad (1.50)$$

An equation governing the moment of momentum, $\boldsymbol{r}\times\boldsymbol{v}$, is obtained by $\boldsymbol{r}$ cross the momentum equation:

$$\frac{\partial(\rho\varepsilon_{ijk} r_j v_k)}{\partial t} + \partial_p[\rho v_p(\varepsilon_{ijk} r_j v_k)]$$
$$= -\varepsilon_{ijk} r_j \partial_k p + \rho\varepsilon_{ijk} r_j g_k + \varepsilon_{ijk} r_j \partial_p \tau_{pk}\,, \qquad (1.51)$$

where any origin is permitted for $\boldsymbol{r}$.

The vorticity $\boldsymbol{\omega} = \nabla\times\boldsymbol{v}$ is governed by a equation formed by $\nabla\times$ the momentum equation. The equation is

$$\frac{\mathrm{d}\omega}{\mathrm{d}t} = -\omega\nabla\cdot\boldsymbol{v} + \omega\cdot\nabla\boldsymbol{v} + \frac{1}{\rho^2}\nabla\rho\times\nabla p$$
$$-\frac{1}{\rho^2}\nabla\rho\times\nabla\cdot\boldsymbol{\tau} + \frac{1}{\rho}\nabla\times\nabla\cdot\boldsymbol{\tau}\,; \qquad (1.52)$$

a derivation of this equation may be found in [1.1, 2].

1.3.3 Angular Momentum

Conservation of angular momentum is a distinct physical law from linear momentum. The net internal angular momentum per unit mass is $\tilde{\boldsymbol{a}}$. This occurs if the molecules were spinning in a preferred direction. Angular momentum crossing an imaginary surface by molecular transport (diffusion) would produce a surface couple $n_j\Omega_{ji}$. One could also propose an external physical process ρG_i that would impart angular momentum directly to the individual particles. Conservation of total angular momentum, $\boldsymbol{r}\times\boldsymbol{v} + \tilde{\boldsymbol{a}}$, leads to the equation

$$\frac{\partial(\rho\varepsilon_{ijk} r_j v_k + \rho\tilde{a}_i)}{\partial t} + \partial_p[\rho v_p(\varepsilon_{ijk} r_j v_k + \tilde{a}_i)]$$
$$= -\varepsilon_{ijk} r_j \partial_k p + \rho\varepsilon_{ijk} r_j g_k$$
$$+ \partial_p(\varepsilon_{ijk} r_j \tau_{pk}) + \rho G_i + \partial_j \Omega_{jk}\,. \qquad (1.53)$$

Subtracting the moment of the momentum equation derived earlier yields a relation governing internal angular momentum

$$\frac{\partial(\rho\tilde{a}_i)}{\partial t} + \partial_p(\rho v_p\tilde{a}_i) = \varepsilon_{ijk}\tau_{jk} + \rho G_i + \partial_j \boldsymbol{\Omega}_{jk}\,. \qquad (1.54)$$

It is usually assumed that the molecular angular momentum is randomly distributed so that $\tilde{\boldsymbol{a}} = 0$ and $\boldsymbol{G}$ and $\boldsymbol{\Omega}$ are zero. Then $\varepsilon_{ijk}\boldsymbol{\tau}_{jk} = 0$ and $\boldsymbol{\tau}$ must be symmetric. Symmetry of $\boldsymbol{\tau}$ will be assumed in the balance of Sect. 1.1.

1.3.4 Energy

The conservation law for total energy leads to

$$\frac{\partial}{\partial t}\left[\rho\left(e + \frac{1}{2}v^2\right)\right] + \nabla\cdot\left[\rho\left(e + \frac{1}{2}v^2\right)\right]$$
$$= -\nabla\cdot\boldsymbol{q} - \nabla\cdot(\boldsymbol{v}p) + \rho\boldsymbol{v}\cdot\boldsymbol{g} + \nabla\cdot(\boldsymbol{\tau}\cdot\boldsymbol{v})\,. \qquad (1.55)$$

Here the *heat flux* vector $\boldsymbol{q}$ accounts for the transport of energy by microscopic mechanisms.

Subtracting the kinetic energy equation yields the thermal energy

$$\frac{\partial}{\partial t}\rho e + \nabla\cdot(\rho\boldsymbol{v}e) = -\nabla\cdot\boldsymbol{q} - p\nabla\cdot\boldsymbol{v} + \Phi\,. \qquad (1.56)$$

The symbol $\Phi \equiv \tau : \nabla\boldsymbol{v} = \tau_{ij}\partial_j v_i$ represents the viscous dissipation that creates thermal energy from kinetic energy.

The thermal energy equation with temperature as the dependent variable is derived using general thermodynamic relations. It is

$$\rho c_\mathrm{p}(T, p)\frac{\mathrm{d}T}{\mathrm{d}t} = -\nabla\cdot\boldsymbol{q} + \Phi + \beta T\frac{\mathrm{d}p}{\mathrm{d}t}\,. \qquad (1.57)$$

1.3.5 Entropy

The fundamental equation expressing the second law of thermodynamics is

$$\rho\frac{\mathrm{d}s}{\mathrm{d}t} = -\nabla\cdot\frac{\boldsymbol{q}}{T} - \frac{1}{T^2}\boldsymbol{q}\cdot\nabla T + \frac{1}{T}\Phi\,. \qquad (1.58)$$

The terms $-\nabla\cdot\frac{\boldsymbol{q}}{T} - \frac{1}{T^2}\boldsymbol{q}\cdot\nabla T = -\frac{1}{T}\nabla\cdot\boldsymbol{q}$ are written as two terms to separate the reversible $(-\nabla\cdot\frac{\boldsymbol{q}}{T})$ and irreversible $(-\frac{1}{T^2}\boldsymbol{q}\cdot\nabla T)$ effects of heat transfer. The viscous term is irreversible.

1.4 Balance Laws and Global Governing Equations

1.4.1 Regions

Global laws are integrals of the local laws over a chosen region or, on the other hand, may be postulated as basic truths from the start. An arbitrary region, designated as AR, has a specified velocity $\boldsymbol{w}$ at each point on the surface. For a material region, MR, the surface velocity is the local fluid velocity, $\boldsymbol{w} = \boldsymbol{v}$. A fixed region, FR, is one with $\boldsymbol{w} = 0$ everywhere. It is sometimes useful to consider a region with a surface velocity that is constant in space $\boldsymbol{w} = \boldsymbol{W}(t)$. Such a region has a constant volume and is designated VR. The fluid velocity relative to the VR is

$$\boldsymbol{u} = \boldsymbol{v} - \boldsymbol{W} \,. \tag{1.59}$$

A region enclosing a rocket and following it through space is a volume region, VR. The velocity of the rocket is $\boldsymbol{W}(t)$ and the rocket engine discharges gases from the region.

Elementary thermodynamic texts do not have a uniform notation for regions. The arbitrary region (AR) defined above might be called an *open system*, a *deformable control volume*, a *control volume*, or some combination of these terms. The fixed region (FR) defined above might be called an *open system*, or simply a *control volume*. The material region might be called a *system*, a *constant mass system*, or a *closed system*.

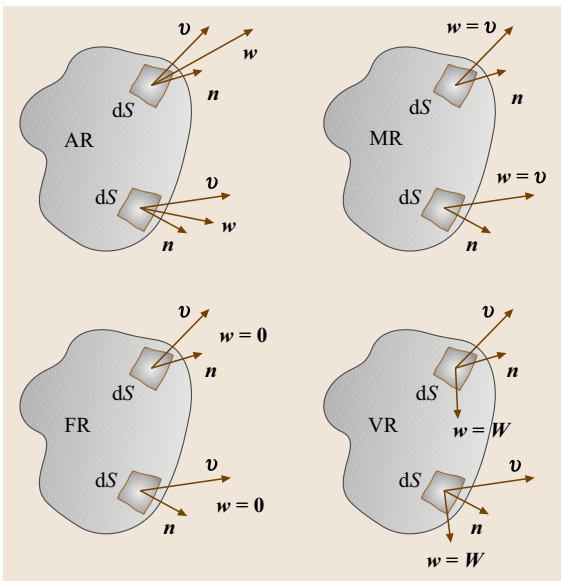

Fig. 1.1 AR, arbitrary region with $\boldsymbol{w}$ prescribed; MR, material region with $\boldsymbol{w}$ equal the local fluid velocity $\boldsymbol{v}$; FR, fixed region with $\boldsymbol{w}$ equal zero; VR, volume region with $\boldsymbol{w}$ equal to a constant in space $\boldsymbol{W}(t)$

1.4.2 Leibnitz and Gauss Theorems

For a region with arbitrary surface velocity $\boldsymbol{w}$, the Leibnitz theorem is

$$\frac{\mathrm{d}I_{ij}}{\mathrm{d}t} = \frac{\mathrm{d}}{\mathrm{d}t}\int\limits_{V_{\mathrm{AR}}} f_{ij}(x_k,t)\,\mathrm{d}V = \int\limits_{\mathrm{AR}} \frac{\partial f_{ij}(x_k,t)}{\partial t}\,\mathrm{d}V + \int\limits_{\mathrm{AR}} n_m w_m f_{ij}(x_k,t)\,\mathrm{d}S \,, \tag{1.60}$$

and the Gauss theorem is

$$\int\limits_{V_{\mathrm{AR}}} \partial_i f_{jk}(x_l,t)\,\mathrm{d}V = \int\limits_{\mathrm{AR}} n_i f_{jk}(x_k,t)\,\mathrm{d}S \,. \tag{1.61}$$

A global law is derived by letting f_{ij} in the Leibnitz theorem be the quantity of interest in the local equation, substituting the local equation for $\partial f_{ij}/\partial t$ and converting as many volume integrals as possible into surface integrals by the Gauss theorem.

1.4.3 Volume

The volume of the region changes with time according to

$$\frac{\mathrm{d}V_{\mathrm{AR}}}{\mathrm{d}t} = \int\limits_{\mathrm{AR}} \boldsymbol{n}\cdot\boldsymbol{w}\,\mathrm{d}S \,. \tag{1.62}$$

Here $\boldsymbol{n}\cdot\boldsymbol{w}$ is the normal velocity of the surface of the control region.

1.4.4 Mass

Conservation of mass for an arbitrary region is

$$\frac{\mathrm{d}M_{\mathrm{AR}}}{\mathrm{d}t} = \frac{\mathrm{d}}{\mathrm{d}t}\int\limits_{\mathrm{AR}} \rho\,\mathrm{d}V = -\int\limits_{\mathrm{AR}} \boldsymbol{n}\cdot(\boldsymbol{v}-\boldsymbol{w})\,\rho\,\mathrm{d}S \,. \tag{1.63}$$

Here all velocities are absolute velocities with respect to an inertial frame. For a material region, *MR*, $\boldsymbol{v} = \boldsymbol{w}$, and (1.63) becomes $\frac{\mathrm{d}M_{\mathrm{MR}}}{\mathrm{d}t} = \frac{\mathrm{d}}{\mathrm{d}t}\int_{\mathrm{MR}} \rho\,\mathrm{d}V = 0$.

For a volume region, *VR*, with fluid velocity $\boldsymbol{u}$ with respect to the moving region;

$$\frac{\mathrm{d}M_{\mathrm{VR}}}{\mathrm{d}t} = -\int\limits_{\mathrm{VR}} \boldsymbol{n}\cdot\boldsymbol{u}\rho\,\mathrm{d}S \,. \tag{1.64}$$

In the rocket example the mass changes because of the relative velocity of the gases leaving the rocket motor.

1.4.5 Linear Momentum

For an arbitrary region

$$\frac{\mathrm{d}}{\mathrm{d}t}\int_{\mathrm{AR}}(\rho\boldsymbol{v})\,\mathrm{d}V = -\int_{\mathrm{AR}}\rho\boldsymbol{n}\cdot(\boldsymbol{v}-\boldsymbol{w})\,\boldsymbol{v}\,\mathrm{d}S + \int_{\mathrm{AR_{solid}}}\boldsymbol{n}\cdot\boldsymbol{T}\,\mathrm{d}S + \int_{\mathrm{AR_{fluid}}}\boldsymbol{n}\cdot\boldsymbol{\tau}\,\mathrm{d}S - \int_{\mathrm{AR_{fluid}}}\boldsymbol{n}p\,\mathrm{d}S + \int_{\mathrm{AR_{fluid}}}\rho\boldsymbol{F}_g\,\mathrm{d}V\,. \tag{1.65}$$

Moving volume region

$$\frac{\mathrm{d}}{\mathrm{d}t}\int_{\mathrm{VR}}(\rho\boldsymbol{u})\,\mathrm{d}V + M_{\mathrm{VR}}\frac{\mathrm{d}\boldsymbol{W}}{\mathrm{d}t} = -\int_{\mathrm{VR}}\rho(\boldsymbol{n}\cdot\boldsymbol{u})\boldsymbol{u}\,\mathrm{d}S + \int_{\mathrm{VR_{solid}}}\boldsymbol{n}\cdot\boldsymbol{T}\,\mathrm{d}S + \int_{\mathrm{VR_{fluid}}}\boldsymbol{n}\cdot t\,\mathrm{d}S - \int_{\mathrm{VR_{fluid}}}\boldsymbol{n}p\,\mathrm{d}S + \int_{\mathrm{VR_{fluid}}}\rho\boldsymbol{F}_g\,\mathrm{d}V\,. \tag{1.66}$$

Recall that he fluid velocity relative to the VR is $\boldsymbol{u} = \boldsymbol{v} - \boldsymbol{W}$.

1.4.6 Total Energy

For the global energy equations the surface integrals are split into regions where the surface cuts a solid and where it cuts a fluid. Shaft work arises from solid surfaces that are cut by the control surface. Work of a rotating shaft, which involves the tangential velocity, v_t, or translating shaft, which involves the normal velocity, v_n, is described by this term.

$$\dot{W}_{\mathrm{Shaft}} = \int_{\text{Solid surfaces}}(\boldsymbol{n}\cdot\boldsymbol{T})\cdot\boldsymbol{v}\,\mathrm{d}S = \int_{\text{Solid surfaces}}(\boldsymbol{n}\cdot\boldsymbol{T})\cdot(\boldsymbol{v}_n+\boldsymbol{v}_t)\,\mathrm{d}S = \dot{W}_{\text{Shaft normal}} + \dot{W}_{\text{Shaft rotary}}\,. \tag{1.67}$$

In fluid regions the stress tensor is decomposed into pressure and viscous parts,

$$T_{ij} = -p\delta_{ij} + \tau_{ij}\,. \tag{1.68}$$

The total energy equation is

$$\begin{aligned}\frac{\mathrm{d}}{\mathrm{d}t}\int_{\mathrm{AR}}\rho\left(\mathrm{e}+\frac{1}{2}v^2+gZ\right)\mathrm{d}V &= -\int_{\mathrm{AR}}\rho\boldsymbol{n}\cdot(\boldsymbol{v}-w)\left(e+\frac{1}{2}v^2+gZ\right)\mathrm{d}S \\ &\quad + \dot{W}_{\text{Shaft normal}} + \dot{W}_{\text{Shaft rotary}} \\ &\quad + \int_{\text{Fluid surfaces}}(\boldsymbol{n}\cdot\boldsymbol{\tau})\cdot\boldsymbol{v}\,\mathrm{d}S \\ &\quad - \int_{\text{Fluid surfaces}}p\boldsymbol{n}\cdot\boldsymbol{v}\,\mathrm{d}S - \int_{\mathrm{AR}}\boldsymbol{n}\cdot\boldsymbol{q}\,\mathrm{d}S\,.\end{aligned} \tag{1.69}$$

This equation can be expressed in many forms. A popular form is to introduce the concepts of moving boundary work and flow work for the pressure work term.

$$\begin{aligned}&-\int_{\text{Fluid surfaces}}\rho\boldsymbol{n}\cdot\boldsymbol{v}\left(\frac{p}{\rho}\right)\mathrm{d}S \\ &= -\int_{\text{Fluid surfaces}}\rho\boldsymbol{n}\cdot(\boldsymbol{v}-\boldsymbol{w})\left(\frac{p}{\rho}\right)\mathrm{d}S \\ &\quad -\int_{\text{Fluid surfaces}}\rho\boldsymbol{n}\cdot\boldsymbol{w}\left(\frac{p}{\rho}\right)\mathrm{d}S \\ &= \dot{W}_{\text{Flow work}} + \dot{W}_{\text{Boundary work}}\,.\end{aligned} \tag{1.70}$$

Inserting these concepts into (1.69) allows the flow work to be incorporated into the convective term and the enthalpy, $h = e + p/\rho$ to be identified.

$$\begin{aligned}\frac{\mathrm{d}}{\mathrm{d}t}\int_{\mathrm{AR}}\rho\left(\mathrm{e}+\frac{1}{2}v^2+gZ\right)\mathrm{d}V &= -\int_{\mathrm{AR}}\rho\boldsymbol{n}\cdot(\boldsymbol{v}-\boldsymbol{w})\left(h+\frac{1}{2}v^2+gZ\right)\mathrm{d}S \\ &\quad + \dot{W}_{\text{Shaft normal}} + \dot{W}_{\text{Shaft rotary}} \\ &\quad + \dot{W}_{\text{Boundary}} + \int_{\text{Fluid surfaces}}(\boldsymbol{n}\cdot\boldsymbol{\tau})\cdot\boldsymbol{v}\,\mathrm{d}S \\ &\quad - \int_{\mathrm{AR}}\boldsymbol{n}\cdot\boldsymbol{q}\,\mathrm{d}S\,.\end{aligned} \tag{1.71}$$

1.4.7 Thermal Energy

The global thermal energy equation may be found by integrating the local thermal energy equation

$$\begin{aligned}&\frac{\mathrm{d}}{\mathrm{d}t}\int\limits_{\mathrm{AR}}\rho e\,\mathrm{d}V\\&=-\int\limits_{\mathrm{AR}}\rho n_i(v_i-w_i)e\,\mathrm{d}S\\&\quad+\int\limits_{\mathrm{AR}}\tau_{ij}\partial_i v_j\,\mathrm{d}V-\int\limits_{\mathrm{AR}}n_i q_i\,\mathrm{d}S\\&\quad+\int\limits_{\mathrm{AR}}p\partial_i v_i\,\mathrm{d}V\,.\end{aligned}\tag{1.72}$$

1.4.8 Mechanical Energy

Subtracting the thermal energy from the total energy yields the final general form for the compressible flow in an arbitrary region. Here the total head $(1/2v^2+gZ+p/\rho)$ appears. Note that some disciplines reserve the term *head* for items with the dimension of length, i.e., $(1/2gv^2+Z+p/g\rho)$

$$\begin{aligned}&\frac{\mathrm{d}}{\mathrm{d}t}\int\limits_{\mathrm{AR}}\rho\left(\frac{1}{2}v^2+gZ\right)\mathrm{d}V\\&=-\int\limits_{\mathrm{AR}}\rho\boldsymbol{n}\cdot(\boldsymbol{v}-\boldsymbol{w})\left(\frac{1}{2}v^2+gZ+\frac{p}{\rho}\right)\mathrm{d}S\\&\quad+\dot{W}_{\mathrm{Shaft\ normal}}+\dot{W}_{\mathrm{Shaft\ rotary}}+\dot{W}_{\mathrm{Boundary}}\\&\quad+\int\limits_{\text{Fluid surfaces}}(\boldsymbol{n}\cdot\boldsymbol{\tau})\cdot\boldsymbol{v}\,\mathrm{d}S\\&\quad+\int\limits_{\mathrm{AR}}\Phi\,\mathrm{d}V-\int\limits_{\mathrm{AR}}p\nabla\cdot\boldsymbol{v}\,\mathrm{d}V\end{aligned}\tag{1.73}$$

The term representing viscous dissipation is usually replaced by defining a head loss h_l.

$$\begin{aligned}\dot{m}gh_l&\equiv\int\limits_{FR}\tau_{ij}\partial_i v_j\,\mathrm{d}V\\&=\int\limits_{FR}\Phi\,\mathrm{d}V\ \text{ for symmetric }\boldsymbol{\tau}\,.\end{aligned}\tag{1.74}$$

1.4.9 Entropy

An exact expression of the second law of thermodynamics is

$$\begin{aligned}&\frac{\mathrm{d}}{\mathrm{d}t}\int\limits_{\mathrm{AR}}\rho s\,\mathrm{d}V\\&=-\int\limits_{AR}\rho n_i(v_i-w_i)s\,\mathrm{d}S-\int\limits_{AR}\frac{1}{T}n_i q_i\,\mathrm{d}S\\&\quad-\int\limits_{AR}\frac{1}{T^2}q_i\partial_i T\,\mathrm{d}V+\int\limits_{AR}\frac{1}{T}\tau_{ij}S_{ji}\,\mathrm{d}V\,.\end{aligned}\tag{1.75}$$

Here the last two terms are irreversible effects and always positive; neglecting them leads to an inequality well known in thermodynamics.

1.5 Constitutive Equations

Many practically important fluids obey constitutive relations for a Newtonian fluid with Fourier heat conduction. The Newtonian relationship for the stress rate of strain contains two viscosity coefficients

$$\tau_{ij}=\lambda\partial_k v_k\delta_{ij}+2\mu S_{ij}\tag{1.76}$$

Inserting the Stokes assumption, $\lambda=-2\mu/3$, yields

$$\tau_{ij}=-\frac{2}{3}\mu\partial_k v_k\delta_{ij}+2\mu S_{ij}\,.\tag{1.77}$$

The Fourier conduction law is

$$q_i=-\kappa\partial_i T\tag{1.78}$$

For completeness Fick´s diffusion law for a binary mixture relates the diffusion flux and the concentration gradient with the binary diffusion coefficient as the proportionality constant.

$$\boldsymbol{j}_{\mathrm{A}}=\rho_{\mathrm{A}}(\boldsymbol{v}_{\mathrm{A}}-\boldsymbol{v})=-\rho\mathcal{D}_{\mathrm{AB}}\nabla x_{\mathrm{A}}\,.\tag{1.79}$$

1.6 Navier–Stokes Equations

The Navier–Stokes equations for a compressible flow may be considered as the continuity equation together with the momentum and energy equations for a Newtonian fluid:

$$\rho\left[\left(\frac{\partial \boldsymbol{v}}{\partial t}+\boldsymbol{v}\cdot\nabla\boldsymbol{v}\right)\right]=-\nabla p+\rho\boldsymbol{g}-\nabla\left(\frac{2}{3}\mu\nabla\boldsymbol{v}\right)+2\nabla(\mu S)\,,$$
$$S\equiv\frac{1}{2}\nabla\boldsymbol{v}+\frac{1}{2}(\nabla\boldsymbol{v})^{\mathrm{T}}\,,$$
$$\rho c_{\mathrm{p}}(T,\,p)\frac{\mathrm{d}T}{\mathrm{d}t}=-\kappa\nabla^2T+\Phi+\beta T\frac{\mathrm{d}p}{\mathrm{d}t}\,. \tag{1.80}$$

1.6.1 Incompressible Flows

For incompressible flows the density is approximately constant and transport coefficients are approximately constant. These are consistent assumptions at low Mach numbers (a characteristic velocity divided by the speed of sound) with adiabatic walls or isothermal walls with small temperature differences. The equations take the form

$$\nabla\boldsymbol{v}=0\,, \tag{1.81}$$
$$\frac{\partial\boldsymbol{v}}{\partial t}+\boldsymbol{v}\cdot\nabla\boldsymbol{v}=-\frac{1}{\rho}\nabla p+\boldsymbol{g}+\nu\nabla\cdot\nabla\boldsymbol{v}\,,$$
$$\nabla\cdot\nabla\boldsymbol{v}=\nabla^2\boldsymbol{v}\,, \tag{1.82}$$
$$\frac{\mathrm{d}\omega}{\mathrm{d}t}=-\boldsymbol{\omega}\cdot\nabla\boldsymbol{v}+\nu\nabla^2\boldsymbol{v}\,. \tag{1.83}$$

Two related equations govern the enstrophy and the pressure:

$$\frac{\mathrm{d}}{\mathrm{d}t}\left(\frac{1}{2}\omega^2\right)=\omega_i\omega_jS_{ji}+\nu\partial_j\partial_j\left(\frac{1}{2}\omega^2\right)-\nu\partial_j\omega_i\partial_j\omega_i\,, \tag{1.84}$$
$$\frac{1}{\rho}\nabla^2p=\boldsymbol{v}\cdot\nabla^2\boldsymbol{v}+\boldsymbol{\omega}\cdot\boldsymbol{\omega}-\nabla^2\left(\frac{1}{2}v^2\right)\,. \tag{1.85}$$

1.7 Discontinuities in Density

1.7.1 Normal Surface Discontinuity

Consider a surface discontinuity in the fluid. This might be thought of as a region with a finite thickness in the limit as the thickness approaches zero. The surface moves with velocity $\boldsymbol{W}$. Figure 1.2 is a typical example that depicts a shock wave caused by a blunt body moving at supersonic speed with respect to the surrounding fluid. Fluid on one side is called fluid A and that on the other fluid B. The unit normal vector $\boldsymbol{n}_{\mathrm{A}}$ points from the discontinuity into fluid A, and $\boldsymbol{n}_{\mathrm{B}}$ points from the discontinuity into fluid B. Assume that there is no mass, momentum or energy within the discontinuity and that the tangential velocity component is unchanged, $\boldsymbol{v}_{\mathrm{At}}=\boldsymbol{v}_{\mathrm{Bt}}$. The mass flow across the discontinuity is conserved.

$$\rho_{\mathrm{A}}\boldsymbol{n}_{\mathrm{A}}\cdot(\boldsymbol{v}_{\mathrm{A}}-\boldsymbol{W})+\rho_B\boldsymbol{n}_B\cdot(\boldsymbol{v}_B-\boldsymbol{W})=0\,. \tag{1.86}$$

The normal vectors may be replaced, $\boldsymbol{n}_{\mathrm{A}}=-\boldsymbol{n}_{\mathrm{B}}=\boldsymbol{n}$. The tangential momentum equation yields a balance of shear forces.

$$(\boldsymbol{n}_{\mathrm{A}}\cdot\tau_{\mathrm{A}})_{\mathrm{t}}+(\boldsymbol{n}_{\mathrm{B}}\cdot\tau_{\mathrm{B}})_{\mathrm{t}}=0\,. \tag{1.87}$$

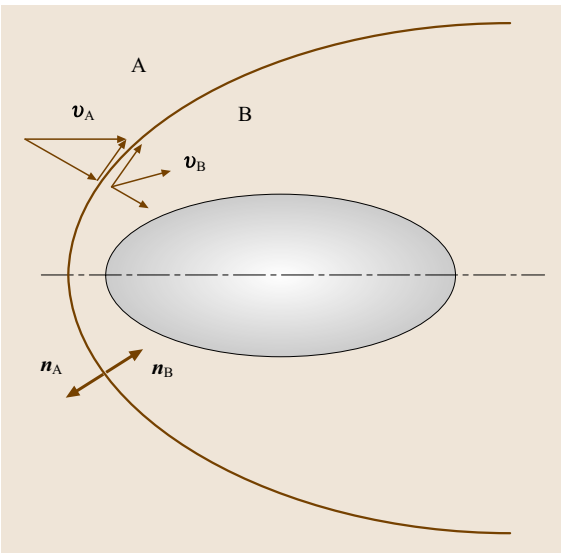

Fig. 1.2 Discontinuity across a shock wave. The tangential velocity is unchanged. The normal velocity is decreased

Let the normal component of the fluid velocity be $\boldsymbol{n}_{\mathrm{A}}\cdot\boldsymbol{v}_{\mathrm{A}}=v_{\mathrm{A}n}$. The normal direction momentum equa-

tion is

$$[\rho_A \cdot \boldsymbol{n}_A(\boldsymbol{v}_A - \boldsymbol{W})v_{An} + p_A - \boldsymbol{n}_A \cdot (\boldsymbol{n}_A \cdot \boldsymbol{\tau}_A)] + \boldsymbol{n}_B \cdot [\rho_B \boldsymbol{n}_B \cdot (\boldsymbol{v}_B - \boldsymbol{W})v_{Bn} + p_B - \boldsymbol{n}_B \cdot (\boldsymbol{n}_B \cdot \boldsymbol{\tau}_B)] = 0 . \quad (1.88)$$

If e_t is the total (kinetic plus internal) energy, conservation of energy requires that

$$[\rho_A e_{tA} \boldsymbol{n}_A \cdot (\boldsymbol{v}_A - \boldsymbol{W})\boldsymbol{v}_{An} + p_A \boldsymbol{v}_{An} - \boldsymbol{n}_A \cdot (\boldsymbol{\tau}_A \cdot \boldsymbol{v}_A) + \boldsymbol{n}_A \cdot \boldsymbol{q}_A] + [\rho_B e_{tB} \boldsymbol{n}_B \cdot (\boldsymbol{v}_B - \boldsymbol{W})\boldsymbol{v}_{Bn} + p_B \boldsymbol{v}_{Bn} - \boldsymbol{n}_B \cdot (\boldsymbol{\tau}_B \cdot \boldsymbol{v}_B) + \boldsymbol{n}_B \cdot \boldsymbol{q}_B] = 0 . \quad (1.89)$$

Because the discontinuity surface contains no mass, the curvature and the time dependence of $\boldsymbol{W}$ have no effect on the local validity of the equations above.

1.7.2 Fluid–Solid Boundary

The central issue here is the condition on the tangential velocity. In many situations the viscous no-slip condition is adequate. However, some situations require a more-refined approach. The analysis above covers the case of a porous or vaporizing wall without slip. Let u_s be the slip velocity of the fluid along the wall. Slip is often expressed as a slip length, defined as

$$\beta = \frac{u_s}{\mathrm{d}u/\mathrm{d}y|_0} = \frac{u_s}{\dot{\gamma}} , \quad (1.90)$$

$$\dot{\gamma} \equiv \mathrm{d}u/\mathrm{d}y|_0 . \quad (1.91)$$

Because the interactions of gasses with solids and liquids with solids are different, these fluids must be dealt with separately.

In gases an important parameter is the Knudsen number, which compares the mean free path length λ with the flow length scale h:

$$\mathrm{Kn} = \frac{\lambda}{h} = \sqrt{\frac{\gamma\pi}{2}}\frac{M}{\mathrm{Re}} . \quad (1.92)$$

The relation with the Mach and Reynolds numbers is often useful. A first-order equation (derived from kinetic theory) for the slip is Maxwell's equation.

$$u_s = \frac{2 - \sigma_v}{\sigma_v}\mathrm{Kn}h\dot{\gamma} . \quad (1.93)$$

Here σ_v is the tangential momentum accommodation coefficient. The Knudsen number becomes large for a large object in a rarefied gas, or a very small object at atmospheric pressure.

Slip in liquids is only observed at small scales. The slip length is on the order on 100 nm (0.1 μm) Experimental results have been correlated as a power law

$$\beta = A\dot{\gamma}^B ,$$
$$u_s = A\dot{\gamma}^{B+1} . \quad (1.94)$$

The constant B is about 1/2. Unfortunately, the dimensions in the constants in the expressions above interact. Changing B changes the dimensions of A. More-detailed comments are in Chap. 19.

1.7.3 Interfaces with Surface Tension

Interfaces with two thermodynamic phases or immiscible substances may require that we postulate a surface tension property. Surface tension, force per length, is the two-dimensional world analogue to pressure. However, it is taken as a thermodynamic property of the substances and the temperature. The curvature of the surface is important. Let R_1 and R_2 be the principle radii of curvature of the surface. The curvature is

$$2\mathcal{H} = -\left(\frac{1}{R_1} + \frac{1}{R_2}\right) . \quad (1.95)$$

Conservation of mass leads to the same equation as for normal discontinuities. The momentum equation contains two surface tension effects. One effect is from the curvature of the surface and another from a possible variation of the surface tension along the surface.

$$\rho\boldsymbol{n} \cdot (\boldsymbol{v}_A - \boldsymbol{w})\boldsymbol{v}_A - \rho\boldsymbol{n} \cdot (\boldsymbol{v}_B - \boldsymbol{w})\boldsymbol{v}_B = [\boldsymbol{n} \cdot \boldsymbol{\tau}_A - \boldsymbol{n}p_A] - [\boldsymbol{n} \cdot \boldsymbol{\tau}_B - \boldsymbol{n}p_B] - \nabla_{(s)}\boldsymbol{\sigma} - \boldsymbol{\sigma}\boldsymbol{n}2\mathcal{H} . \quad (1.96)$$

Surfaces without mass crossing the interface have simplified expressions. In addition to the unit vector $\boldsymbol{n}$ normal to the surface, let the vectors $\boldsymbol{b}$ and $\boldsymbol{t}$ be orthogonal unit vectors within the surface. The momentum equations in these three directions are

$$\boldsymbol{n}\text{-direction} : 0 = (\boldsymbol{\tau}_{nn_A} - \boldsymbol{\tau}_{nn_B}) - [p_A - p_B] - 2\sigma\mathcal{H} , \quad (1.97)$$

$$\boldsymbol{n}\text{-direction} : 0 = (\boldsymbol{\tau}_{ntA} - \boldsymbol{\tau}_{ntB}) - \frac{d\sigma}{\mathrm{d}t} , \quad (1.98)$$

$$\boldsymbol{b}\text{-direction} : 0 = (\boldsymbol{\tau}_{nbA} - \boldsymbol{\tau}_{nbB}) - \frac{d\sigma}{db} . \quad (1.99)$$

Contact lines, where two surfaces meet, require special treatment and if the contact line moves slip is required.

1.8 Constitutive Equations and Nonlinear Rheology of Polymer Melts

Constitutive equations describing the nonlinear rheological behavior of polymer melts have been a subject of focus due to their importance in designing and optimizing polymer processing as well as their analytical role in providing a logical picture of the molecular structure of the polymer. They are also needed to obtain closed system of the continuity and momentum equations describing flow of such materials. Constitutive equations can be classified according to their scale of work (continuum mechanics or microstructural), their method of formulation (integral or differential), or according to their approach towards time-deformation separability (separable or nonseparable) [1.3]. Most of the current theoretical work in rheology is devoted to the development of precise constitutive equations with parameters that are in some way or other obtainable through the microstructural properties of polymer melts and solutions as well as other non-Newtonian fluids. The present chapter presents an overview of the constitutive equations derived from continuum mechanics, and their evolution to the development of microstructural integro-differential equations.

Among the microstructural constitutive equations for polymer solutions and melts, the tube model has proven to be successful in predicting the linear rheological behavior of linear polymer melts and solutions, but is incapable of predicting the strain hardening behavior observed both in linear and in long-chain branched melts [1.4]. The continuum-based models, on the other hand, are merely phenomenological definitions of the solution or melt behavior and provide little or no information on the structure of the polymer molecule. It is the goal of this chapter to set the boundaries of the most recent microstructural constitutive equations and discuss the potentials of tackling the yet unsolved problems in nonlinear rheology of polymer melts.

Most recent developments which are based on modifications of the tube model have resulted in considerable progress in nonlinear viscoelastic theories and can predict strain hardening in linear polydisperse polymer melts with reasonable quantitative precision [1.5, 6]. However, a significant discrepancy arises when comparing the strain hardening of linear polydisperse melts to that of long-chain branched polymer melts since the latter show a considerably steeper onset of strain hardening [1.7, 8]. Reversing double-step strain measurements reveal another difference in melt behaviors since long-chain branched melts exhibit totally reversible behavior of the Kay-Bernstein–Kearsley–Zapas (K-BKZ) type up to considerable large deformations, whereas polydisperse linear polymers show early irreversible deformations [1.9].

In the present chapter we will discuss the main features of the evolution from the classical constitutive equations based on continuum mechanics to the microstructural theories which were developed in recent years. It is emphasized that in the present chapter, the rheological constitutive equations for concentrated polymer solutions and melts are in focus. In addition, in Sect. 1.2 and Sect. 1.3 of the handbook a number of rheological constitutive equations for slurries, gels, suspensions and emulsions is introduced and discussed in detail.

1.8.1 Classical Theories

The General Viscous Fluid

The main concern of many practical computational problems, e.g., in polymer processing is to find a suitably formulated method to calculate the flow rate. In this case and under certain circumstances the elasticity effects (and consequently the normal stress behavior in simple shear flow) may be neglected. Assuming incompressibility, and that the stress tensor $\boldsymbol{\sigma}$ only depends on the instantaneous condition of the rate of deformation tensor $\boldsymbol{D}$ (and not on its time derivatives), and assuming that the extra stress tensor $\boldsymbol{\tau} = \boldsymbol{\sigma} + p\boldsymbol{I}$ and $\boldsymbol{D}$ be coaxial (i. e., they have the same directions of principal axes), the state of stress can be described by:

$$\boldsymbol{\sigma} = -p\boldsymbol{I} + 2\eta\,(II_{\mathrm{D}}, III_{\mathrm{D}})\,\boldsymbol{D}\,, \tag{1.100}$$

where II_{D} and III_{D} are the second and third invariants of the rate of deformation tensor. (The first invariant I_{D} is zero due to the assumption of incompressibility.)

Clearly, (1.100) reduces to the Newtonian fluid provided $\eta = \eta_0$ is independent of the invariants of $\boldsymbol{D}$:

$$\boldsymbol{\sigma} = -p\boldsymbol{I} + 2\eta_0\boldsymbol{D}\,. \tag{1.101}$$

For simple shear flows, the third invariant III_{D} vanishes identically. It is commonly assumed that III_{D} is not very important in other flows, and hence it is customary to omit the dependence on III_{D}, leading to the standard form of the general viscous fluid:

$$\boldsymbol{\sigma} = -p\boldsymbol{I} + 2\eta\,(II_{\mathrm{D}})\,\boldsymbol{D}\,. \tag{1.102}$$

The later equation allows a three-dimensional representation of scalar deformation-rate-dependent flow laws.

A popular form of such flow laws has been proposed by *Ostwald* and *de Waele* [1.3]:

$$\eta = m I I_{\mathrm{D}}^{(n-1)/2} , \tag{1.103}$$

hence:

$$\boldsymbol{\sigma} = -p\boldsymbol{I} + 2m I I_{\mathrm{D}}^{(n-1)/2}\boldsymbol{D} , \tag{1.104}$$

where m is a temperature-dependent parameter and n determines whether the fluid is shear thinning ($n < 1$) or shear thickening ($n > 1$). However, like most phenomenological constitutive equations, (1.104) is only valid for a certain range of shear rates and fails at small shear rates. Experimental observations suggest that the viscosity finally reaches a (Newtonian) plateau at lower shear rates whereas (1.104) predicts infinite values for n<1. Other models to compensate for this shortcoming such as *Carreau–Yasuda model* [1.3],

$$\frac{\eta - \eta_\infty}{\eta_0 - \eta_\infty} = \frac{1}{(1 + \lambda^a |I I_{\mathrm{D}}|)^{\frac{n-1}{a}}} \tag{1.105}$$

are in use, but their application needs a choice of extra parameters that yield no insight into the microstructural aspects of the fluid.

The Rubber-Like Liquid Theory

Based on early observations of rubber elasticity, *Lodge* [1.10] proposed a polymer melt to be a network of temporary junctions or entanglements that are created

1. at a constant rate independent of deformation or deformation rate;
2. in an isotropic state even under deformation.

This, along with the assumption of affine deformation led to the rubber-like liquid constitutive equation for the stress tensor $\boldsymbol{\sigma}$ in the form

$$\boldsymbol{\sigma} = -p\boldsymbol{I} + \int_{-\infty}^{t} \left[m(t-t')\boldsymbol{C}_t^{-1}(t')\right] \mathrm{d}t' , \tag{1.106}$$

where p denotes the isotropic pressure contribution, $\boldsymbol{C}_t^{-1}(t')$ is the relative Finger strain tensor and $\boldsymbol{I}$ is the unit tensor. The memory function $m(t-t')$, which for simplicity is often expressed by a discrete relaxation spectrum (g_i, λ_i) [1.9],

$$m(t-t') = \sum_{i=1}^{N} \frac{g_i}{\lambda_i} \mathrm{e}^{-(t-t')/\lambda_i} , \tag{1.107}$$

is the time derivative of the relaxation modulus $G(t)$

$$m(t-t') = \frac{\partial G(t-t')}{\partial t'} . \tag{1.108}$$

The discrete relaxation modes g_i and λ_i are free parameters of the theory, and have to be determined by suitable linear viscoelastic experiments. Based on the concept of reptation [1.4], considerable progress has been made in recent years in relating $G(t)$ to molar mass, molar mass distribution, and topology (linear or branched) of polymer melts, but its numerical precision depends on numerous model assumptions, especially in the case of randomly long-chain branched melts [1.11, 12]. This makes the experimental determination from dynamic mechanical analysis still the most reliable method to obtain $m(t-t')$ Chap. 9.

Later it was shown that the rubber-like liquid equation fails at large deformations [1.13], and severely overpredicts the stresses of polymer melts. This will be discussed in the following section when introducing the evolution of the K-BKZ-type constitutive equations.

K-BKZ and Related Equations

A large group of rheological equations of state for nonlinear viscoelastic behavior can be deduced as special cases of the K-BKZ equation [1.14].

The generalized relation between stress and finite strain for rubber elasticity is:

$$\boldsymbol{\sigma} = f(\boldsymbol{B}) = -p\boldsymbol{I} + g_1(I, II)\boldsymbol{B} + g_2(I, II)\boldsymbol{B} , \tag{1.109}$$

where $\boldsymbol{B} = \boldsymbol{B}_n(t)$ is the Green deformation tensor describing the deformation from the natural, stress-free state $t' = n$ to the deformation state at time t, and the relation to the relative Finger strain tensor is given by

$$\boldsymbol{B}_n(t) = \boldsymbol{C}_t^{-1}(n) . \tag{1.110}$$

The functions g_1 and g_2 are material functions of the first and second invariant of $\boldsymbol{B}$ or $(\boldsymbol{C}^{-1})$,

$$I = I_B = \mathrm{tr}(\boldsymbol{B}) \tag{1.111}$$

and

$$II = II_B = \frac{1}{2}\left[I_B^2 - \mathrm{tr}(\boldsymbol{B}^2)\right] . \tag{1.112}$$

The values of invariants of the Green (and Finger) tensor for shear, uniaxial, equibiaxial and planar deformations are summarized in Table 1.1.

If the stress can be derived from an energy potential $W(I, II)$, the rubber is called hyperelastic. In the case of time-dependent viscoelastic materials, this concept can be generalized to an energy potential $w(I, II, t-t')$, which depends not only on the invariants I and II of the relative Finger tensor $\boldsymbol{C}_t^{-1}(t')$, but also on the time

difference $t-t'$. The strain energy W is then given by

$$W = \int_{-\infty}^{t} [w(I, II, t-t')]\,\mathrm{d}t' \,. \tag{1.113}$$

From W, the K-BKZ equation is then derived as [1.14]:

$$\boldsymbol{\sigma} = -p\boldsymbol{I} + \int_{-\infty}^{t} \left(2\frac{\partial w}{\partial I}\boldsymbol{C}^{-1} - 2\frac{\partial w}{\partial II}\boldsymbol{C}\right) \mathrm{d}t' \,, \tag{1.114}$$

$\boldsymbol{C} = \boldsymbol{C}_t(t')$ is called the relative Cauchy tensor. By choosing a suitable potential w, (1.114) can be adapted to describe the time-dependent deformation behavior of a general viscoelastic material. Separating the effects of time and deformation will lead to a separable K-BKZ equation of the form:

$$\boldsymbol{\sigma} = -p\boldsymbol{I} + \int_{-\infty}^{t} m(t-t') \left(h_1\boldsymbol{C}^{-1} + h_2\boldsymbol{C}\right) \mathrm{d}t' \,. \tag{1.115}$$

If the functions $h_1(I, II)$ and $h_2(I, II)$ are not expressible as derivatives of a potential, (1.115) is called a separable Rivlin–Saywers equation [1.3], although the term K-KBZ equation is often (wrongly) also used in this case. The rubber-like liquid theory of Lodge mentioned in the previous section is recovered from (1.115) with h_1 and h_2 being equal to 1 and 0, respectively, and w is given by

$$w(I, II, t-t') = m(t-t')\,(I-3) \,. \tag{1.116}$$

The main problem is now reduced to obtaining a reasonable expression for w for real polymer melts in a wide range of deformations and deformation rates, a task that remained largely elusive.

However, nonlinear shear and extensional stress growth experiments on many polymer melts for sufficiently large deformations proved time-deformation separability to be valid [1.3]. This, along with neglecting the relative Cauchy tensor by setting $h_2 = 0$ in (1.109) led to the so-called Wagner I equation [1.3, 15–17]:

$$\boldsymbol{\sigma} = -p\boldsymbol{I} + \int_{-\infty}^{t} m(t-t')h(I, II)\boldsymbol{C}^{-1}\,\mathrm{d}t' \,, \tag{1.117}$$

where $h(I, II) \le 1$ is called the damping function, which expresses the survival probability of network strands regarding nonlinear deformations [1.16, 17]. A first approximation proposed for the damping function was:

$$h(II_\mathrm{B}) = \mathrm{e}^{-\sqrt{II-3}} \,, \tag{1.118}$$

which, for unidirectional shear flows, will lead to the simplified form:

$$h(\gamma) = \mathrm{e}^{-n\gamma} \,. \tag{1.119}$$

Using the fitting exponent $n = 0.143$ for low-density polyethylene (LDPE) melts, (1.119) performs quite well for shear deformations as large as $\gamma = 13$. For larger deformations a combination of two exponential functions of the form

$$h(\gamma) = a\,\mathrm{e}^{-n_1\gamma} + (1-a)\,\mathrm{e}^{-n_2\gamma} \,, \tag{1.120}$$

was suggested, which extended the predictable deformation range up to $\gamma = 30$ [1.15].

However, comparison to experimental evidence has shown that recoverable deformations, e.g.in reversing shear or elastic recoil experiments [1.18–20], are overpredicted by the Wagner I equation. In order to overcome this defect, the damping function was replaced by a functional $H(t, t')$ of the deformation (the so-called Wagner II equation [1.3]),

$$\boldsymbol{\sigma} = -p\boldsymbol{I} + \int_{-\infty}^{t} m(t-t')H(t, t')\boldsymbol{C}^{-1}\,\mathrm{d}t' \,. \tag{1.121}$$

The functional was chosen in such a way that it always behaves as a decreasing function [1.18, 21],

$$H(t, t') = \min\,[h(I, II)] \,. \tag{1.122}$$

Using this functional and a linear combination of the strain invariants,

$$L = \alpha I + (1-\alpha)\,II \,, \tag{1.123}$$

and a damping function $h(L)$ of the form

$$h(L) = a\,\mathrm{e}^{-n_1\sqrt{L-3}} + (1-a)\mathrm{e}^{-n_2\sqrt{L-3}} \,, \tag{1.124}$$

reasonable quantitative agreement between theory and experiment for the nonlinear behavior both in shear and

Table 1.1 First and second invariants of the Green or Finger tensor in terms of the shear strain γ and Hencky strain ε

Type of flow	I	II
Simple shear	$3+\gamma^2$	$3+\gamma^2$
Uniaxial	$\mathrm{e}^{2\varepsilon}+2\mathrm{e}^{-\varepsilon}$	$2\mathrm{e}^{\varepsilon}+\mathrm{e}^{-2\varepsilon}$
Equibiaxial	$\mathrm{e}^{-2\varepsilon}+2\mathrm{e}^{\varepsilon}$	$2\mathrm{e}^{-\varepsilon}+\mathrm{e}^{2\varepsilon}$
Planar	$1+\mathrm{e}^{-2\varepsilon}+\mathrm{e}^{2\varepsilon}$	$1+\mathrm{e}^{2\varepsilon}+\mathrm{e}^{-2\varepsilon}$

uniaxial extensional flow of many industrial (polydisperse) polymer melts could be obtained by the use of four nonlinear material parameters. Later *Papanastasiou* et al. proposed a damping function of the following sigmoidal form [1.22]

$$h(I, II) = \frac{\alpha}{(\alpha - 3) + \beta\, I + (1 - \beta)\, II} \,. \tag{1.125}$$

The Wagner I and II equations have the disadvantage of neglecting the second normal stress difference in shear flow, which in reality is small and negative, but nonzero. This is related to the fact that the experimentally derived strain functions summarized so far cannot be generalized to other types of deformations, even if they perform well in predicting the melt behavior under a certain flow regime. Samarkus et al. have exemplified this problem by showing that the coefficients of Wagner II equation obtained by shearing experiments could not predict planar extensional behavior [1.23].

For the Doi–Edwards model [1.4], to be discussed in detail in Sect. 1.8.3 of this chapter, a simple analytical approximation for the corresponding potential w (the so-called Currie approximation [1.24]) was found,

$$w \approx \frac{5}{2} \ln\left(\frac{J-1}{7}\right) \,, \tag{1.126}$$

with a generalized invariant J

$$J = I + 2\sqrt{II + \frac{13}{4}} \,. \tag{1.127}$$

This leads to

$$h_1 = \frac{5}{J-1}, \quad h_2 = \frac{-2h_1}{J-I} \,, \tag{1.128}$$

thereby predicting a negative second normal stress difference in shear flow. However, as the Doi–Edwards model does not account for chain stretching (Sect. 1.8.3), the predictive power of (1.128) concerning the rheology of industrially important polydisperse polymer melts is limited.

Finally, Wagner and Demarmels proposed an ansatz for the two strain functions h_1 and h_2 which represents a special form of a Rivlin–Sawyers equation describing a wide range of deformation types [1.25]. Starting with the ratio β of second (N_2) to first (N_1) normal stress differences from a shear experiment,

$$\beta = \frac{N_1}{N_2} = \frac{h_2}{h_1 - h_2} \,, \tag{1.129}$$

which coincides with the corresponding relation for the normal stresses in planar experiments and was assumed to be strain-independent, they proposed

$$\begin{aligned} h_1 &= (1+\beta)\; h\,(I, II) \,, \\ h_2 &= \beta\, h\,(I, II) \,, \\ h\,(I, II) &= \left[1 + a\sqrt{(I-3)\,(II-3)}\right]^{-1} \,, \end{aligned} \tag{1.130}$$

which resulted in good agreement with experimental data in uniaxial, biaxial and planar deformations of a polydisperse isobutene melt.

Despite their qualitative success in describing the polymer melt behavior, constitutive equations based on classical continuum mechanics lack insight into the relation between rheology and the structure of polymers and cannot be used as predictive tools. This calls for a better understanding of the microstructure of polymer melts, subject of the following section, to develop more realistic, yet feasible models.

1.8.2 Convected Derivatives and Differential Equations

A major part of the differential constitutive equations consists of generalizations of the Maxwell model and possesses the character of continuum formulations based merely on phenomenological observations. The Maxwell model was initially utilized to describe the behavior of viscoelastic materials in the linear deformation range by considering a viscoelastic material to behave as a linear combination of a spring with spring constant g and a dashpot with constant viscosity η_0. The scalar stress σ in the material then obeys the linear first-order differential equation:

$$\boldsymbol{\sigma} + \lambda \dot{\boldsymbol{\sigma}} = \eta_0 \dot{\gamma} \,, \tag{1.131}$$

where $\dot{\gamma}$ is the scalar shear rate, and $\lambda = \eta_0/g$ is the relaxation time. (1.131) can be generalized to the three-dimensional case and to large deformations,

$$\boldsymbol{\sigma} + \lambda \overset{\nabla}{\boldsymbol{\sigma}} = 2\eta_0 \boldsymbol{D} \,, \tag{1.132}$$

by introduction of the *upper convected derivative* of the stress tensor $\overset{\nabla}{\sigma}$ as

$$\overset{\nabla}{\boldsymbol{\sigma}} = \dot{\boldsymbol{\sigma}} - (\nabla \boldsymbol{v})^T \cdot \boldsymbol{\sigma} - \boldsymbol{\sigma} \cdot (\nabla \boldsymbol{v}) \,. \tag{1.133}$$

This description solves the problem of frame invariance by introducing a frame of reference that is *convected* and deformed with material lines.

The upper convective Maxwell model (1.132), is the one-mode differential equivalent of Lodge's (1.106) with an exponentially fading memory. Both integral and

differential versions of Lodge's equation were successful in providing a qualitative prediction of the primary normal stress difference in shear and strain hardening in extension. Replacing the upper convective derivative in (1.126) by the *lower convected* form,

$$\overset{\triangle}{\boldsymbol{\sigma}} = \dot{\boldsymbol{\sigma}} - (\nabla \boldsymbol{v}) \cdot \boldsymbol{\sigma} - \boldsymbol{\sigma} \cdot (\nabla \boldsymbol{v})^{\mathrm{T}} \,, \tag{1.134}$$

the lower convective Maxwell model is obtained. In the integral version, this is equivalent to replacing the Finger strain tensor by the Cauchy tensor $\boldsymbol{C}$ as the deformation measure in (1.106) with the exponentially fading memory. The lower convective Maxwell model predicts a negative second normal stress difference of the same magnitude as the first normal stress difference in shear and no strain hardening in extension, which is not in agreement with experiment. It also has no molecular basis. Equation (1.133) and (1.134) are not the only frame-invariant time derivatives. Oldroyd recognized that infinitely many could be constructed, and he proposed generalizations of the convected Maxwell models by allowing for higher-order terms to appear, e.g., in the form of the eight-constant Oldroyd equation, later followed by Giesekus and others. For details the reader is referred to [1.3]. However, experience with these purely continuum-mechanics-based equations teaches that frame invariance itself is not restrictive enough to keep the number of terms manageable, and that some molecular insight is needed.

1.8.3 Microstructural Theories

Theories from Continuum Mechanics and Their Microscopic Equivalents

In microscopic terms, stress in polymeric systems originates from orientation and extension of entropic springs, which can be thought of as e.g.representing molecular strands between entanglements. An isotropic distribution of molecular strands normalized with respect to their equilibrium length can be described by an isotropic distribution of unit vectors $\boldsymbol{u}$. Assuming affine deformation, the inverse relative deformation gradient $\boldsymbol{F}^{-1}$ transforms a unit vector $\boldsymbol{u}$ into a deformed vector $\boldsymbol{u}'$,

$$\boldsymbol{u}' = \boldsymbol{F}^{-1} \cdot \boldsymbol{u} \,. \tag{1.135}$$

The Finger strain tensor can then be expressed as

$$\boldsymbol{C}^{-1} = 3\langle \boldsymbol{u}'\boldsymbol{u}' \rangle \tag{1.136}$$

where $\langle \ldots \rangle$ denotes an integral over an isotropic distribution of unit vectors before deformation,

$$\langle \ldots \rangle = \frac{1}{4\pi} \int \ldots \, \mathrm{d}\Omega \,, \tag{1.137}$$

where $\mathrm{d}\Omega$ is an infinitesimal solid angle, and the integration is over the surface of a unit sphere. This is depicted schematically in Fig. 1.3.

A similar scheme can be used to find a microscopic representation of the Cauchy strain tensor $\boldsymbol{C}$: If $\boldsymbol{n}$ represents an isotropic distribution of unit surfaces, and if these are assumed to be deformed affinely, the deformation gradient $\boldsymbol{F}$ transforms a unit surface vector $\boldsymbol{n}$ into the deformed surface vector $\boldsymbol{n}'$,

$$\boldsymbol{n}' = \boldsymbol{n} \cdot \boldsymbol{F} \,. \tag{1.138}$$

The Cauchy strain tensor $\boldsymbol{C}$ can then be expressed as

$$\boldsymbol{C} = 3\langle \boldsymbol{n}'\boldsymbol{n}' \rangle \,. \tag{1.139}$$

Considering further that the invariants I and II are equivalent to

$$I = 3\langle u'^2 \rangle \,, \tag{1.140}$$

$$II = 3\langle n'^2 \rangle \,, \tag{1.141}$$

where u' and n' represent the lengths of the vectors $\boldsymbol{u}'$ and $\boldsymbol{n}'$ respectively,

$$u' = \sqrt{\boldsymbol{u}' \cdot \boldsymbol{u}'} \,,$$
$$n' = \sqrt{\boldsymbol{n}' \cdot \boldsymbol{n}'} \,, \tag{1.142}$$

the separable Rivlin–Sawyers (1.115) can be expressed in microscopic terms as:

$$\boldsymbol{\sigma} = -p\boldsymbol{I} + \int_{-\infty}^{t} m(t-t') \Big[H_1\big(\langle u'^2 \rangle, \langle n'^2 \rangle\big) \langle \boldsymbol{u}'\boldsymbol{u}' \rangle + H_2\big(\langle u'^2 \rangle, \langle n'^2 \rangle\big) \langle \boldsymbol{n}'\boldsymbol{n}' \rangle \Big] \mathrm{d}t' \tag{1.143}$$

where the strain functions H_1 and H_2 converge to $H_1 + H_2 = 3$ in the linear viscoelastic limit [1.9].

However, while (1.143) expresses the strain measure in terms of the primitive quantities $\boldsymbol{u}$ and $\boldsymbol{n}$, it is by no means guaranteed that this is the most appropriate representation of the strain measure when taking into

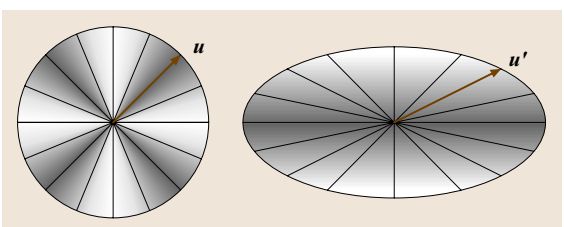

Fig. 1.3 Affine deformation of unit vectors: graphic representation of the Finger strain tensor

account topological constraints of the macromolecular chains.

The Tube Model of Doi and Edwards (DE)

The kinetic theory of *Doi* and *Edwards* [1.4] models intermolecular interaction for concentrated systems of monodisperse linear polymer chains by the tube concept: the mesh of constraints caused by surrounding chains confines the molecular chain laterally to a tube-like region. Relaxation occurs by two mechanisms: *chain retraction* by equilibration along the tube contour, which is supposed to be a fast process governed by the Rouse time τ_R of the chain with τ_R proportional to the square of the molar mass, and *chain diffusion* by reptation out of the tube with a reptation or disengagement time τ_d proportional to the third power of the molar mass. As for high values of the molar mass, chain retraction is fast compared to chain diffusion, this model explains naturally the experimentally observed time-deformation separability of the nonlinear relaxation modulus for times greater than the equilibration time.

Assuming that the diameter of the tube is not changed by deformation, or equivalently that the tension in the deformed polymer chain is equal to its equilibrium value, Doi and Edwards derived [by use of the independent alignment assumption (IAA)] a single integral constitutive equation of the form [1.4]:

$$\boldsymbol{\sigma} = -p\boldsymbol{I} + \int_{-\infty}^{t} m(t-t')\boldsymbol{S}_{\mathrm{DE}}^{\mathrm{IA}}\left(t,t'\right)\,\mathrm{d}t' \,. \tag{1.144}$$

Here, $\boldsymbol{S}_{\mathrm{DE}}^{\mathrm{IA}}$ denotes the strain measure of the Doi–Edwards (DE) model with the independent alignment assumption,

$$\boldsymbol{S}_{\mathrm{DE}}^{\mathrm{IA}} = \frac{15}{3}\left\langle \frac{\boldsymbol{u}'\boldsymbol{u}'}{u'^2}\right\rangle = 5\boldsymbol{S}\,, \tag{1.145}$$

where $\boldsymbol{S} = \boldsymbol{S}(t,t')$ is the relative second-rank orientation tensor, and $\boldsymbol{u}'$ denotes deformed unit vectors according to (1.135). The DE model with the independent alignment assumption assumes that stress is created by an affine rotation of tube segments.

A rigorous derivation for stress relaxation after a step deformation leads to a somewhat different strain measure,

$$\boldsymbol{S}_{\mathrm{DE}} = \frac{15}{4}\frac{1}{\langle u'\rangle}\left\langle \frac{\boldsymbol{u}'\boldsymbol{u}'}{u'}\right\rangle \tag{1.146}$$

and to a nonlinear integro-differential equation for the stress tensor in general flows. However, the strain measure $\boldsymbol{S}_{\mathrm{DE}}$ is often used simplistically instead of $\boldsymbol{S}_{\mathrm{DE}}^{\mathrm{IA}}$ in the single integral (1.144).

$\boldsymbol{S}_{\mathrm{DE}}^{\mathrm{IA}}$ and $\boldsymbol{S}_{\mathrm{DE}}$ produce different predictions for the second normal stress difference (with $\boldsymbol{S}_{\mathrm{DE}}^{\mathrm{IA}}$ being in better agreement with available experimental data), and consequently also different predictions in biaxial deformations, whereas their difference seems to be negligible for the case of uniaxial extension [1.26].

For monodisperse polymer melts and solutions, the Doi–Edwards strain measures seem to give an acceptable description of material behavior in step-shear experiments for times greater than the equilibration time. For fast deformations (as defined below) and for polydisperse linear and branched polymer melts, on the other hand, although time-deformation separability often works over most or even the entire (experimentally attainable) time range, the measured stresses in shear and extensional flows are often much higher than predicted by the Doi–Edwards strain measure [1.3, 13, 27, 28].

Models with Pre-averaged Chain Stretch

The DE Theory with Chain Stretch. The DE theory, despite its deficiency in predicting chain stretch, established the theoretical foundation for further studies on nonlinear deformations of polymer melts.

The DE constitutive equation in shear is applicable only to deformation rates $\dot{\gamma}$ that are smaller than the reciprocal Rouse time τ_R of the chain, i. e., for flows with Deborah numbers $\mathrm{De} = \dot{\gamma}\tau_R < 1$. The first attempt to generalize the DE equation for faster flows was by applying a pre-averaged stretch ratio into the DE constitutive equation when DE > 1 [1.4, 29]. Assuming the equilibrium chain length to be $\bar{L}$ and its value at time t

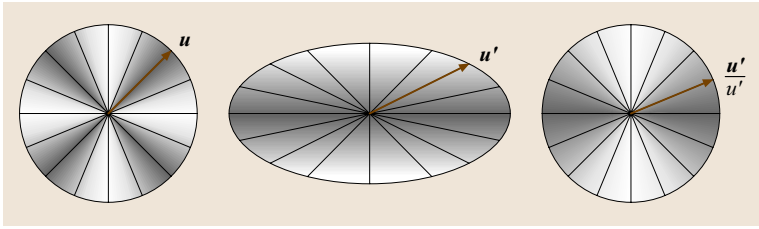

Fig. 1.4 The DE theory with independent alignment assumption (IAA): the stress tensor is the result of a mere change in chain orientation, sometimes called an *affine rotation*

to be $L(t)$, the stress tensor is given by

$$\boldsymbol{\sigma} = -p\boldsymbol{I} + \frac{G_N^0}{\bar{L}^2}\left\langle \int_0^{L(t)} \mathrm{d}sL(t)\,(\boldsymbol{uu})\right\rangle , \tag{1.147}$$

where $\boldsymbol{u} = \boldsymbol{u}(s,t)$ describes the orientation at time t of a chain segment at position s along the chain, and the average is taken over all chains of the system. For fast deformations, this can be approximated by

$$\begin{aligned}\boldsymbol{\sigma} &= -p\boldsymbol{I} + \frac{G_N^0}{\bar{L}^2}\left\langle \int_0^{L(t)} \mathrm{d}sL(t)\,(\boldsymbol{uu})\right\rangle \\ &\approx -p\boldsymbol{I} + G_N^0\left(\frac{L(t)}{\bar{L}}\right)^2\left\langle \frac{1}{L(t)}\int_0^{L(t)} \mathrm{d}s\,(\boldsymbol{uu})\right\rangle \\ &= -p\boldsymbol{I} + G_N^0\left(\frac{L(t)}{\bar{L}}\right)^2 \bar{\boldsymbol{S}}(t)\,,\end{aligned} \tag{1.148}$$

where $\bar{\boldsymbol{S}}$ represents the orientation tensor of the ensemble of chains. Equation (1.148) turns into an exact relation for step-strain deformations.

Equation (1.148) is then approximated by a single integral equation with the stretch ratio $\lambda = (L(t)/\bar{L})$ left outside the integration,

$$\begin{aligned}\boldsymbol{\sigma}(t) &= -p\boldsymbol{I} + \lambda^2(t)\int_{-\infty}^{t} m(t-t')\boldsymbol{S}_{\mathrm{DE}}(t,t')\,\mathrm{d}t' \\ &= -p\boldsymbol{I} + \frac{15}{4}\lambda^2(t)G_N^0\bar{\boldsymbol{S}}(t)\,.\end{aligned} \tag{1.149}$$

We call this the DE equation with pre-averaged chain stretch. It created the need to develop a proper evolution equation for $\lambda(t)$. This was proposed for the first time by *Pearson* et al. [1.29] by noticing that the rate of chain stretch can be obtained by assuming a balance between the frictional force on the chain, and the spring force created in the chain by stretching,

$$\xi\left(\boldsymbol{\kappa}:\bar{\boldsymbol{S}}L - \frac{\mathrm{d}L}{\mathrm{d}t}\right) = \frac{3k_{\mathrm{B}}T}{\bar{L}^2}(L-\bar{L})\,, \tag{1.150}$$

where ξ is the friction coefficient, and the first term on the left hand side of (1.150) represents an affine deformation; $\boldsymbol{\kappa} = \nabla\boldsymbol{v}$ is the velocity-gradient tensor, k_{B} Boltzmann's constant and T temperature. By dividing by the equilibrium length $\bar{L}$ and introducing the Rouse time, $\tau_{\mathrm{R}} = kM^2$, this leads to an evolution equation for the stretch $\lambda(t)$ of the form:

$$\frac{\mathrm{d}\lambda}{\mathrm{d}t} = \boldsymbol{\kappa}:\bar{\boldsymbol{S}}\lambda - \frac{1}{\tau_{\mathrm{R}}}(\lambda-1)\,. \tag{1.151}$$

Noticing the fact that the chain cannot undergo infinite elongation, another restriction was later added to (1.151) by assuming an upper level of chain stretch, $\lambda_{\max}$. This led to modifying the right hand side of (1.151) in a fashion that would accommodate this requirement [1.30]:

$$\frac{\mathrm{d}\lambda}{\mathrm{d}t} = \boldsymbol{\kappa}:\bar{\boldsymbol{S}}\lambda - \frac{1}{\tau_{\mathrm{R}}}(\lambda-1)\,c(\lambda)\,, \tag{1.152}$$

with

$$c(\lambda) = \frac{\lambda_{\max}}{\lambda_{\max}-\lambda}\,. \tag{1.153}$$

The newly introduced parameter $\lambda_{\max}$ determines the finite stretching limit of the chain and is reported by *Fang* et al. to be between 3 and 6 depending on the polymer system considered [1.31]. The latter work also introduces an alternative for $c(\lambda)$ in (1.153) by assuming a new $c(\lambda)$ that is derived from an entropy expression,

$$c(\lambda) = \frac{3Z\lambda_{\max}^2(\lambda+1)}{\lambda\left(\lambda_{\max}^2-\lambda^2\right)}\,, \tag{1.154}$$

where Z is the number of entanglement segments per chain. This led to somewhat better agreement with experimental data for shear experiments, but it offers only qualitative agreement with experimental results for start-up and steady-state values of extensional viscosities.

The Pom-Pom Model. The concept of a pre-averaged chain stretch was further used by *McLeish* and *Larson* [1.32] to account for the nonlinear rheology of a multi-arm model polymer initially proposed by *McLeish* [1.33]. The so-called pom-pom model is an extension of an H-shaped molecule having a backbone of molecular weight M_a and q arms of molecular weight M_{b} at each end (the only branching points on the backbone). The backbone is assumed to be stretched by the deformation until the tension in the backbone equals the sum of the equilibrium tensions of the dangling arms, which occurs when $\lambda = q$. Figure 1.5 shows schematically a typical pom-pom molecule and the process of backbone stretch and branch retraction into the tube of the backbone for a large enough deformation.

In the simplified version of the model [1.34], the orientation contribution to the stress from the dangling arms is neglected so that the dominant contribution arises

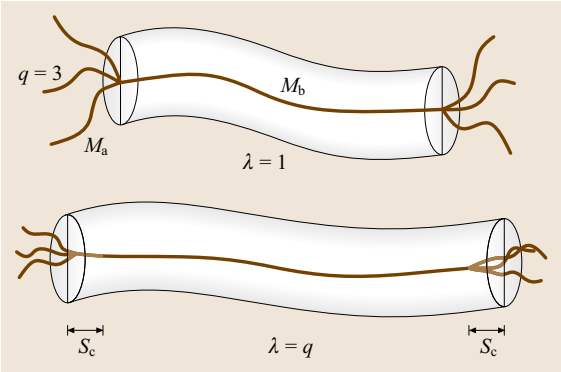

Fig. 1.5 Schematic presentation of a pom-pom molecule

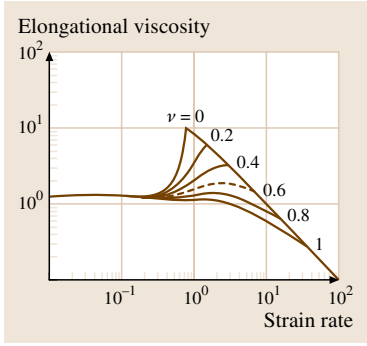

Fig. 1.6 Steady viscosity in uniaxial tension for $0 < \nu < 1$ with pom-pom parameters: $q = 5$, $M_a = 5M_e$ and $M_b = 15M_e$ (after [1.35], with permission)

from the orientation and stretch of the backbone only. The stress tensor is then obtained from (1.149) as:

$$\boldsymbol{\sigma}(t) = -p\boldsymbol{I} + \frac{15}{4}\lambda^2(t)G_N^0\phi_b^2\bar{\boldsymbol{S}}(t)\,, \tag{1.155}$$

where ϕ_b indicates the mass fraction of the backbone. While the evolution of backbone orientation is assumed to be dominated by a single orientation relaxation time τ_b,

$$\bar{\boldsymbol{S}} = \int_{-\infty}^{t} \boldsymbol{\tau}_b^{-1}\, e^{-\frac{t-t'}{\tau_b}}\, \boldsymbol{S}_{DE}(t,t')\,dt'\,, \tag{1.156}$$

backbone stretch depends on a stretch relaxation time τ_s and is derived from a similar stretch evolution equation as given by (1.141) as long as $\lambda < q$,

$$\frac{d\lambda}{dt} = \lambda\boldsymbol{\kappa} : \bar{\boldsymbol{S}} - \frac{1}{\tau_s} f(\lambda)\,, \tag{1.157}$$

while otherwise $\lambda = q$ is assumed. $f(\lambda)$ was originally chosen to have a linear form,

$$f(\lambda) = \lambda - 1\,, \tag{1.158}$$

which causes the steady-state extensional viscosities to undergo a sharp maximum as shown for the case $\nu = 0$ in Fig. 1.6 This was in contrast to experimental results and unrealistic since it suggested a sudden retraction of the arm only at the moment when $\lambda = q$. In fact, relaxation of an arm can have a significant effect on the overall relaxation also before a maximum stretch is reached and very small retractions of the arms into the tube can effectively reduce the drag from the arms. To account for this effect *Blackwell* et al. [1.35] introduced *local branch point displacement* and changed $f(\lambda)$ to

$$f(\lambda) = (\lambda - 1)e^{\nu(\lambda-1)} \quad \text{with } 0 < \nu < 1\,. \tag{1.159}$$

Using this new evolution equation for the backbone stretch, Blackwell et al. showed that a moderate value of ν smoothes the steady-state extensional viscosity plotted against the strain rate, as shown in Fig. 1.6, which is equivalent to a gradual arm retraction instead of an instant withdrawal.

Although the original pom-pom model was introduced by making use of the DE orientation tensor in its integral form (1.146), the orientation tensor was soon approximated by a differential evolution equation [1.32] which would allow more feasible numerical applications. The differential pom-pom equation has entirely overshadowed the original pom-pom idea since its introduction. Although the scope of the present work is integral constitutive equations, we give a short account of the differential version here because of its widespread application in numerical simulations of polymer processing [1.36]. However, we emphasize the fact that the differential approximation departs both quantitatively and qualitatively a great deal from the original pom-pom idea by causing enhanced shear thinning and neglecting the 2nd normal stress difference in shear flow [1.37,38].

The multimode pom-pom model is another prevalent development in the theory introduced by *Inkson* et al. [1.34] in order to account for the multiple branching effects which are present in long-chain branched industrial polymer melts such as LDPE, and which are treated by the concept of the so-called seniority/priority effects. According to this model, each branching is assumed as having further branches on it so that it acts as the backbone of the next branching generation from its other end [1.39]. This leads to the introduction of multiple relaxation times representative of various branching levels, and a stress tensor that is summed over the entire range of relaxation modes. The set of equations of the multimode differential pom-pom model is therefore

$$\text{Stress:} \qquad \boldsymbol{\sigma} = 3\sum_i g_i\lambda_i^2\bar{\boldsymbol{S}}_i\,, \tag{1.160}$$

Orientation: $\bar{\boldsymbol{S}}_i = \dfrac{\boldsymbol{A}_i}{\mathrm{tr}(\boldsymbol{A}_i)}$

$$\frac{\partial}{\partial t}\boldsymbol{A}_i = \boldsymbol{\kappa}\cdot\boldsymbol{A}_i + \boldsymbol{A}_i\cdot\boldsymbol{\kappa}^{\mathrm{T}} - \frac{1}{\tau_{\mathrm{b},i}}\,(\boldsymbol{A}_i - \boldsymbol{I})\ , \tag{1.161}$$

Stretch: $$\frac{d\lambda_i}{\mathrm{d}t} = \lambda_i\boldsymbol{\kappa} : \bar{\boldsymbol{S}}_i - \frac{1}{\tau_{\mathrm{s},i}}(\lambda_i - 1)\,\mathrm{e}^{\nu_i(\lambda_i - 1)} \quad \text{for} \quad \lambda \le q_i\ . \tag{1.162}$$

Here, for *each relaxation mode* i, four unknown parameters are required. These parameters are:

- *Backbone orientation time*: $\tau_{\mathrm{b},i}$;
- *Fractional relaxation modulus*: g_i ;
- *Number of pom-pom arms*: q_i ;
- *Backbone stretch orientation time*: $\tau_{\mathrm{s},i}$.

While $\tau_{\mathrm{b},i}$ and g_i represent the linear viscoelastic properties of the polymer melt and are obtained from linear viscoelastic experiments, q_i and $\tau_{\mathrm{s},i}$ are nonlinear parameters that are fitted to appropriate nonlinear material functions. This means that for any linear viscoelastic mode, there are two nonlinear parameters.

Figure 1.7 shows results for uniaxial extensional and transient shear viscosities of LDPE International Union of Pure and Applied Chemistry (IUPAC) A. The theoretical curves represent a nine-mode pom-pom as presented by *Inkson* et al. [1.34]. Figure 1.8 shows the nonlinear rheological behavior of a densely branched LDPE modeled with a six-mode pom-pom [1.40].

Further modifications of the differential pom-pom model were proposed by *Verbeeten* et al. [1.41]. By use of a nonlinear, Giesekus-type argument they succeeded in rewriting the pom-pom equation by excluding the finite extensibility condition and the discontinuity associated with it, and introduced a nonzero second normal stress difference. No need to say, this phenomenological description which is also known as the extended pom-pom (XPP) model, despite its computational desirability [1.42], has totally diverted from the original microstructural pom-pom idea and offers little insight into the polymer structure.

Models with Varying Tube Diameter

The original picture of the tube model proved to be a promising and flexible tool for prediction of the rheological behavior of polymer melts. However, as shown in the previous section, assuming a pre-averaged tube stretch will in practice demand numerous simplifying assumptions and a large number of nonlinear parameters as a consequence of pre-averaging. An alternative to circumvent pre-averaging is the assumption of a strain-dependent tube diameter as first suggested by *Marrucci* and *de Cindio* [1.43]. They assumed that the tube is deformed affinely during deformation and the tube volume remains constant, both in contrast to the classical DE theory, which resulted in a single integral constitutive equation of the form

$$\boldsymbol{\sigma} = -p\boldsymbol{I} + \frac{5}{4}\int_{-\infty}^{t} m(t-t')\left\langle\frac{\boldsymbol{u}'\boldsymbol{u}'}{u'}\right\rangle \mathrm{d}t'\ , \tag{1.163}$$

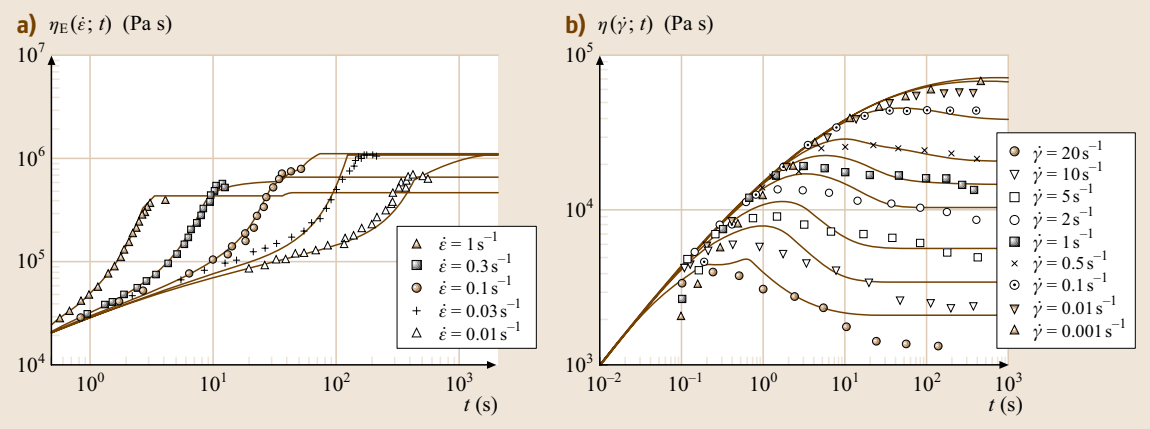

Fig. 1.7a,b Results of a nine-mode pom-pom model analysis for a standard IUPAC LDPE A with molecular weight $M_{\mathrm{w}} = 300\,000$ and molecular weight distribution (MWD) of 17.6 (after [1.34], with permission): **(a)** Elongational viscosity; **(b)** transient shear viscosity

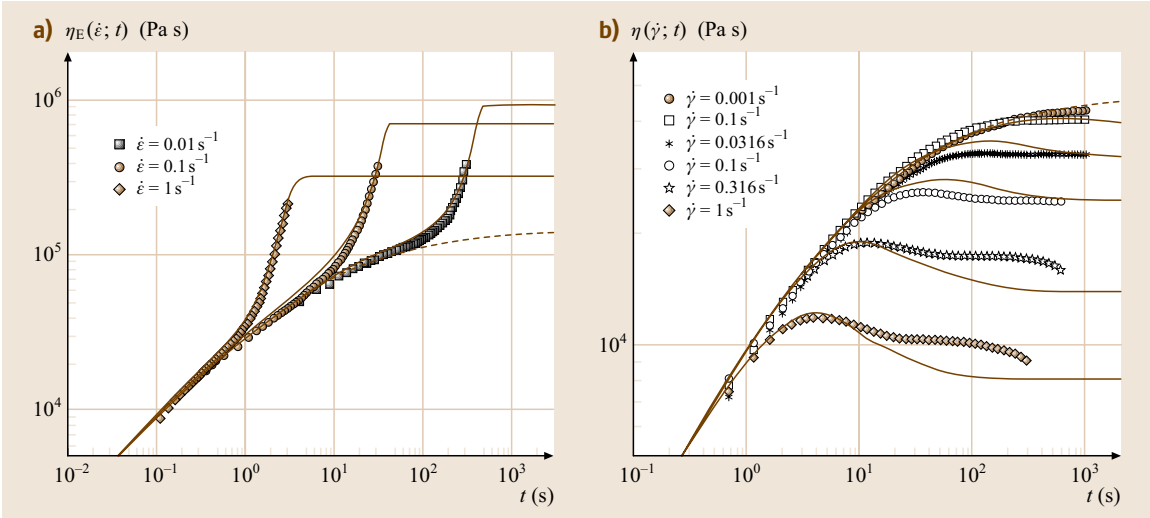

Fig. 1.8a,b Results of a six-mode pom-pom model for an LDPE with $M_w = 235\,500$ and MWD of 17.1 (after [1.40], with permission from Macromolecules 35:10091. Copyright 2002, American Chemical Society): **(a)** elongational viscosity; **(b)** transient shear viscosity

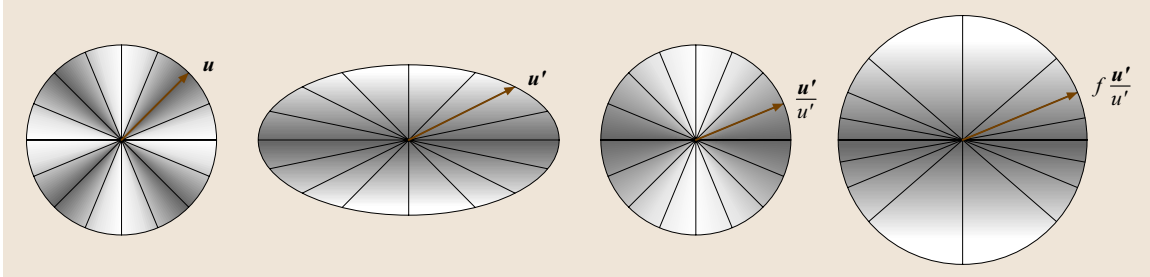

Fig. 1.9 MSF theory: stress is the result of both orientation and isotropic stretch of tube segments by a factor f

which produced better predictions for the extensional behavior of a poly(methyl methacrylate) (PMMA) melt. It was based on their work that Wagner et al. [1.44–47] adopted the concept of varying tube diameter to show that the work of the stress tensor can be correlated to the change of free energy at the molecular scale [1.7].

The Molecular Stress Function (MSF) Model for Linear Melts. In the molecular stress function (MSF) model of Wagner and coworkers [1.7, 44–52], tube stretch is caused by the *squeeze* of the surrounding polymer chains, leading to a reduction of the tube diameter a from its equilibrium value a_0. Taking into account that the tube diameter a represents the mean field of the surrounding chains and its associated strain energy, it is assumed that the tube diameter is independent of the orientation of tube segments. This is depicted schematically in Fig. 1.9.

The stress is then given by

$$\sigma(t) = -p\boldsymbol{I} + \int_{-\infty}^{t} m(t-t')f^2 \boldsymbol{S}_{\mathrm{DE}}^{\mathrm{IA}}(t,t')\,\mathrm{d}t' \,, \quad (1.164)$$

where the molecular stress function f is the inverse of the relative tube diameter,

$$f(t,t') = a_0/a(t,t') \,. \quad (1.165)$$

In contrast to (1.149), the tube stretch in (1.164) does not only depend on the observation time t, but also on the strain history, i. e., for time-dependent strain histories, the tube stretch varies along the tube. The dependence on t and t' is dropped in the following.

Note that while $\boldsymbol{S}_{\mathrm{DE}}^{\mathrm{IA}}$ is related directly to the deformation history via (1.145), no a priori dynamics of the internal variable f is prescribed in the MSF model.

Rather, f^2 is assumed to be directly related to the strain energy stored in the polymeric system, and is determined as solution of an evolution equation derived from an energy balance argument [1.7].

Based on prior work of *de Gennes* [1.53], and *Marrucci* et al. [1.54,55], the molecular stress function f for linear melts is related to a strain-energy function w_{MSF} of the form

$$\frac{w_{\mathrm{MSF}}}{3k_{\mathrm{B}}T} = (f^2 - 1)\,. \tag{1.166}$$

Neglecting dissipative constraint release, i. e., considering the hyperelastic limit, the power input of the stress tensor into the polymer system is equal to the increase of the strain energy by tube deformation [1.7]. f^2 is found as solution of the evolution equation (with velocity gradient $\boldsymbol{\kappa}$ and plateau modulus G_N^0)

$$\frac{1}{3k_{\mathrm{B}}T}\frac{\mathrm{d}w_{\mathrm{MSF}}}{\mathrm{d}t} = \boldsymbol{\kappa} : \frac{\boldsymbol{\sigma}}{5G_N^o} = f^2\,(\boldsymbol{\kappa} : \boldsymbol{S}) \tag{1.167}$$

to be

$$f^2 = \mathrm{e}^{\langle \ln u' \rangle_0}\,, \tag{1.168}$$

i. e., f^2 is an exponential of the orientational free energy $3k_{\mathrm{B}}T\,\langle \ln u' \rangle_0$. $\frac{\mathrm{d}}{\mathrm{d}t}$ indicates the material time derivative.

Note that by use of (1.168), the strain energy function of (1.166) can be expressed as

$$\frac{w_{\mathrm{MSF}}}{3k_{\mathrm{B}}T} = \langle \ln u' \rangle_0 + f^2 - \ln f^2 - 1\,, \tag{1.169}$$

i. e., as the sum of the orientational free energy and the stretch energy. The part of the strain energy due to chain stretch has the desired properties, namely a minimum at equilibrium ($f^2 = 1$) and a quadratic dependence on f in the vicinity of equilibrium.

Predictions of the MSF model are in excellent agreement with the onset of strain-hardening in uniaxial, equibiaxial and planar extension of polydisperse linear polymer melts (the so-called LMSF model), as exemplified in Fig. 1.10 and Fig. 1.11 [1.7].

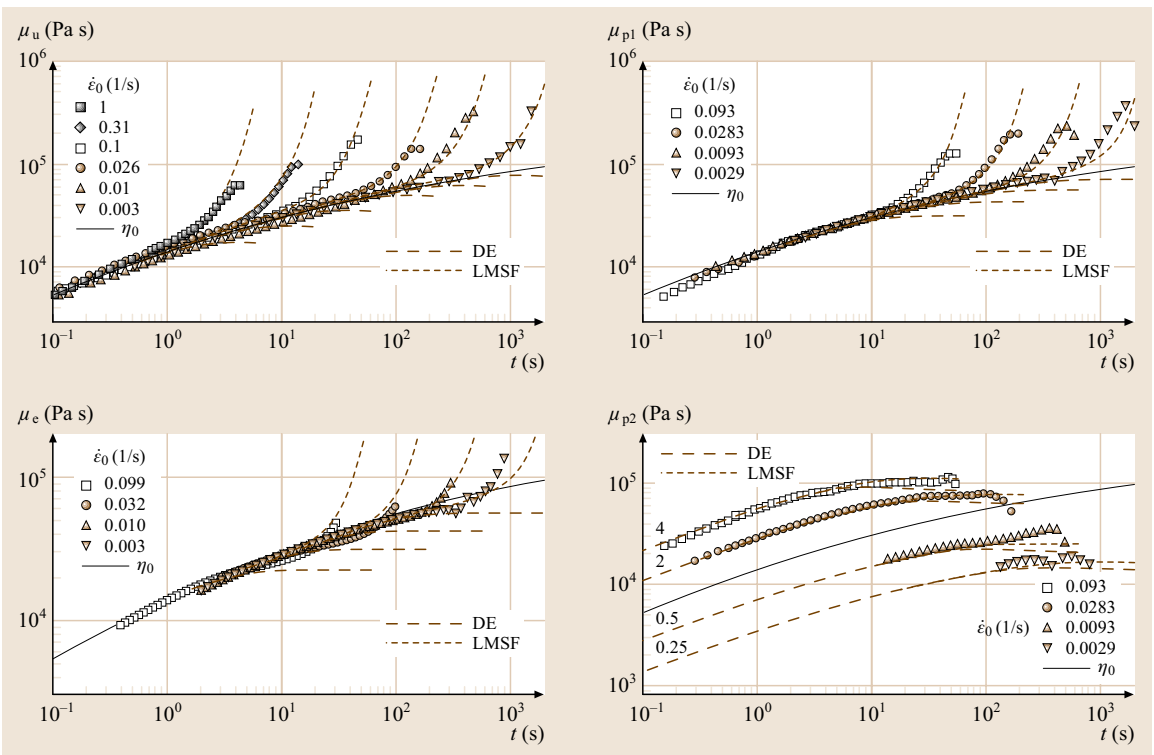

Fig. 1.10 Uniaxial (μ_{u}), equibiaxial (μ_{e}), and planar (μ_{p1}, μ_{p2}) viscosities of a high-density polyethylene (HDPE) at $T = 150\,^{\circ}\mathrm{C}$. Viscosities are normalized with respect to the zero-shear viscosity. Comparison of experimental data (*symbols*) to predictions of DE and LMSF (zero-parameter) models (after [1.7])

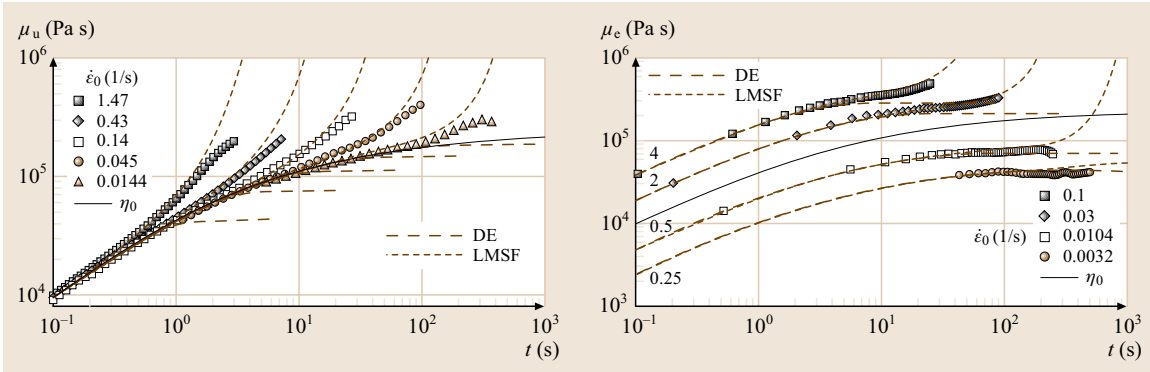

Fig. 1.11 Uniaxial (μ_u) and equibiaxial (μ_e) viscosities of a polystyrene (PS) melt. Viscosities are normalized with respect to the zero-shear viscosity. Comparison of experimental data (*symbols*) to the predictions of the DE and LMSF (zero-parameter) models.

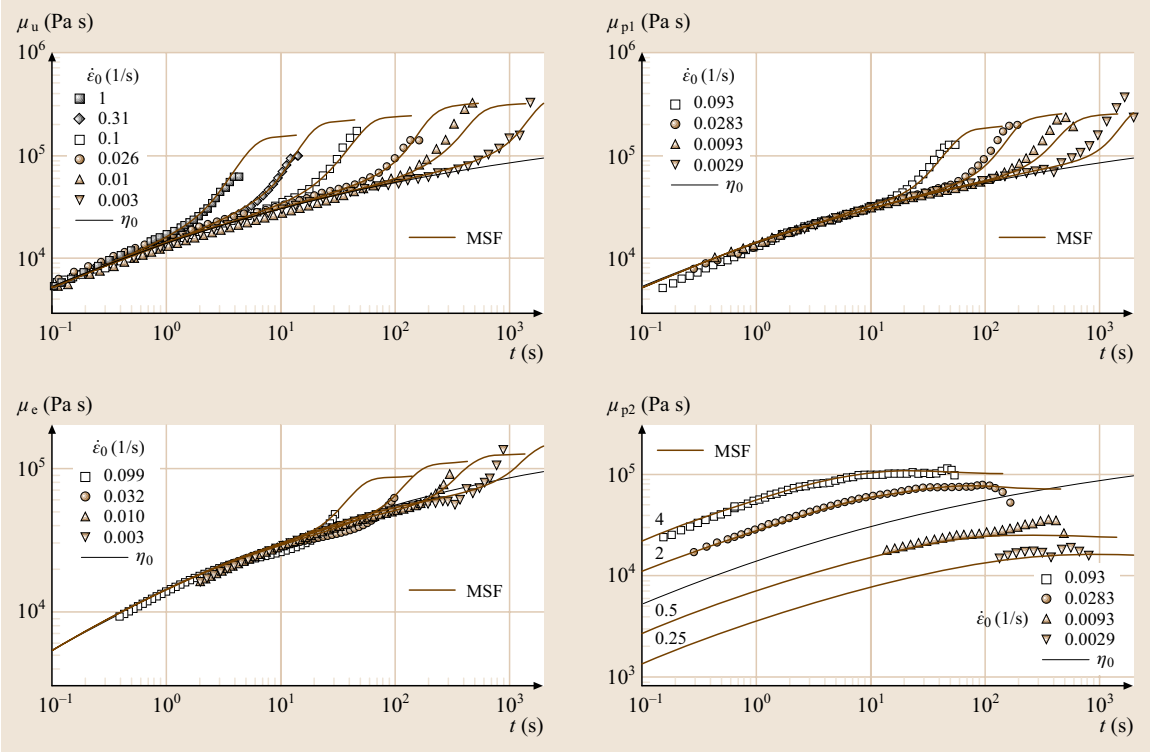

Fig. 1.12 Uniaxial (μ_u), equibiaxial (μ_e), and planar (μ_{p1}, μ_{p2}) viscosities of a HDPE melt. Viscosities are normalized with respect to the zero-shear viscosity. Comparison of experiment to predictions of the MSF model with dissipative constraint release. $f^2_{\max} = 49$ [1.7]

Now dissipative constraint release (CR) is introduced as a dissipative process [1.7], which modifies the energy balance of tube deformation, and leads to a strain-dependent evolution equation for the molecular stress function of the form

$$\frac{\mathrm{d}f^2}{\mathrm{d}t} = f^2\left[(\boldsymbol{\kappa}:\boldsymbol{S}) - \frac{1}{f^2-1}\mathrm{CR}\right] . \qquad (1.170)$$

Constraint release is considered to be the consequence of different convection mechanisms for tube orientation and tube-cross section, and for constant-strain-rate flows can be expressed as

$$\mathrm{CR} = a_1(f^2-1)^2\sqrt{\boldsymbol{D}^2:\boldsymbol{S}} + a_2(f^2-1)^2\sqrt{|\boldsymbol{W}\cdot\boldsymbol{D}:\boldsymbol{S}|} \tag{1.171}$$

with $\boldsymbol{D}$ and $\boldsymbol{W}$ being the rate of deformation and rate of rotation tensor, respectively. The nonlinear material parameters verify $a_1 \geq 0$ and $a_2 \geq 0$. Note that in extensional flows, constraint release depends only on the parameter a_1, while in simple shear flow, both the parameters a_1 and a_2 are of relevance. The evolution equation for the molecular stress function of linear melts in extensional flows is given by

$$\frac{\mathrm{d}f^2}{\mathrm{d}t} = \dot{\varepsilon}f^2\left[S_{11}+mS_{22}-(1+m)S_{33}-a_1(f^2-1)\times\sqrt{S_{11}+m^2S_{22}+(1+m)^2S_{33}}\right] \tag{1.172}$$

where the parameter m $(-1/2 \leq m \leq 1)$ describes the type of extensional flow, and $\dot{\varepsilon}$ is the largest extension rate. S_{ii} are the components of the orientation tensor $\boldsymbol{S}$. At large strains, a maximum $f^2 = f^2_{\max}$ is reached and $\mathrm{d}f^2/\mathrm{d}t = 0$. Hence, the parameter a_1 can be expressed in terms of $f^2_{\max}$ as

$$a_1 = \frac{1}{f^2_{\max}-1}\,; \tag{1.173}$$

$f^2_{\max}$ governs the steady-state value of the viscosity in extensional flows, and corresponds to the maximum of storable elastic energy. It is the only nonlinear material parameter of the theory for describing polymer melt rheology of linear polymers in irrotational flows. The level of agreement between experiments in different extensional deformation modes and theory for a linear polyethylene (PE) melt is demonstrated in Fig. 1.12.

The evolution equation of the molecular stress function for shear flow is given by

$$\frac{\mathrm{d}f^2}{\mathrm{d}t} = \dot{\gamma}f^2\left[S_{12}-\frac{1}{2}\frac{f^2-1}{f^2_{\max}-1}\sqrt{S_{11}+S_{22}} - \frac{a_2}{2}\left(f^2-1\right)\sqrt{|S_{11}-S_{22}|}\right] \tag{1.174}$$

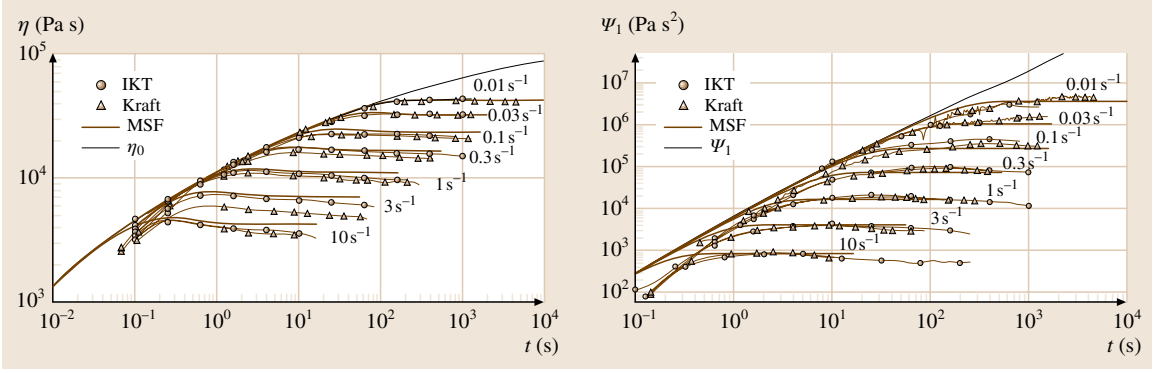

Fig. 1.13 Shear viscosity η and first normal stress function Ψ_1 of a HDPE melt. Comparison of experimental data (*symbols*) to predictions of the MSF model with dissipative constraint release. $f^2_{\max} = 49$ and $a_2 = 2.3$. For details see (after [1.7])

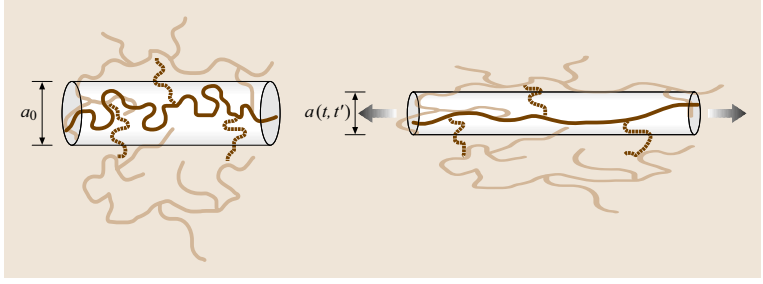

Fig. 1.14 Tube segment of a long-chain branched polymer molecule before and after deformation: one chain segment is stretched, while side-chain segments are compressed [1.49, 50]

and comparison of the predictions to experimental data of the start-up of steady shear flow for the same linear PE melt is shown in Fig. 1.13.

Note that although dissipative constraint release is a rate process, integration of (1.172) and (1.174) leads to a molecular stress function f which is deformation dependent [1.7].

The MSF Model for Long-Chain Branched Melts. The simplest model of a tube section of a long-chain branched macromolecule containing β entanglements consists of one chain segment representing one entanglement oriented in the direction of the tube (the *backbone* of the macromolecule), and one or more side chains representing $\beta - 1$ entanglements (Fig. 1.14). Note that a side chain can contain more than one chain segment, depending on the length of the side chain relative to the entanglement length. Thus, according to this model, chain segments fall into two distinct categories: either they belong to the backbone and are stretched by deformation, or they do not belong to the backbone and are compressed by deformation [1.49].

When the tube is stretched, one segment is extended, while $\beta - 1$ are compressed, leading to a total strain energy of

$$\frac{w_{\mathrm{MSF}}}{3k_{\mathrm{B}}\mathrm{T}} = \frac{1}{\beta}(f^2 - 1) + \frac{(\beta - 1)}{\beta}\left(1 - \frac{1}{f^2}\right) . \quad (1.175)$$

Note that in the vicinity of $f^2 = 1$, this strain energy function is well behaved, as (1.175) (with $\beta = 1$) reduces to (1.166).

The parameter β has values $\beta \geq 1$, with $\beta = 1$ for linear melts. For $\beta = 2$ (the so-called QMSF model), excellent agreement with experimental data of a long-chain branched (radiation-crosslinked) polypropylene (PP) melt is found (Fig. 1.15). Note that the increase in elongational viscosity is steeper for long-chain branched melts than for linear melts.

Introducing again constraint release as a nonlinear dissipative process, which modifies the energy balance of tube deformation, leads to a strain-dependent evolution equation for the molecular stress function of the form

$$\frac{\mathrm{d}f^2}{\mathrm{d}t} = \frac{\beta f^2}{1 + \frac{\beta - 1}{f^4}}\left[(\boldsymbol{\kappa} : \boldsymbol{S}) - \frac{1}{f^2 - 1}\mathrm{CR}\right] . \quad (1.176)$$

The evolution equation for the molecular stress function in constant-strain-rate extensional flows is then

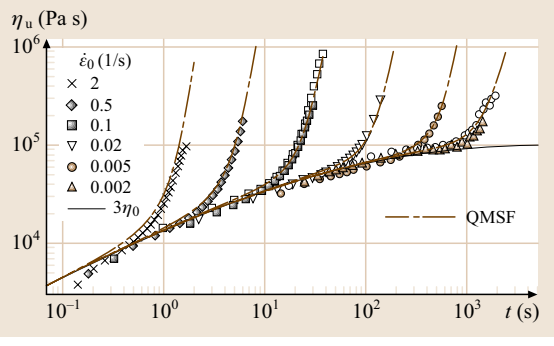

Fig. 1.15 Uniaxial viscosity η_u of a long-chain branched PP melt [1.7]. Comparison of experimental data (*symbols*) to predictions of the MSF model with $\beta = 2$ (QMSF model)

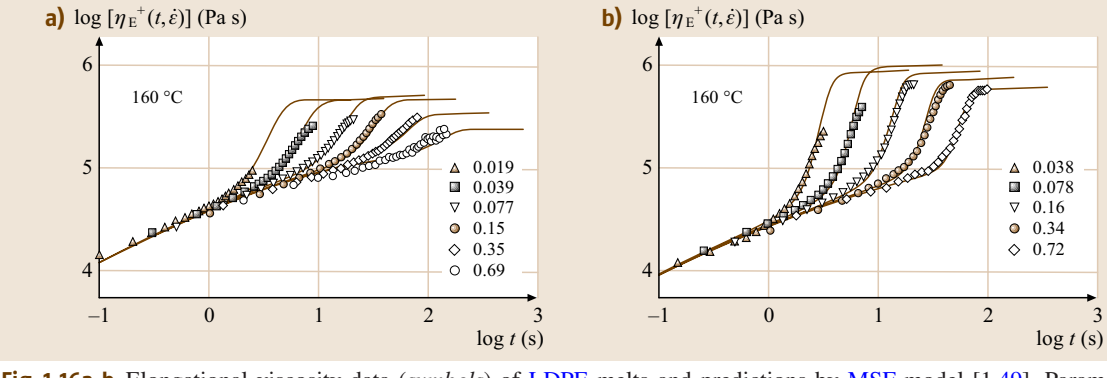

Fig. 1.16a,b Elongational viscosity data (*symbols*) of LDPE melts and predictions by MSF model [1.49]. Parameters indicate elongation rate in units of s^{-1}. **(a)** LDPE produced by tubular process (tubular o): $\beta = 2$ and $f^2_{\max} = 30$; **(b)** LDPE produced by an autoclave process (autoclave O): $\beta = 4$ and $f^2_{\max} = 80$

given by

$$\frac{\mathrm{d}f^2}{\mathrm{d}t} = \dot{\varepsilon}\frac{\beta f^2}{1+\frac{\beta-1}{f^4}}\left[S_{11}+mS_{22}-(1+m)S_{33} - \frac{f^2-1}{f_{\max}^2-1}\sqrt{S_{11}+m^2S_{22}+(1+m)^2S_{33}}\right] \tag{1.177}$$

and in constant-shear-rate flow by

$$\frac{\mathrm{d}f^2}{\mathrm{d}t} = \dot{\gamma}\frac{\beta f^2}{1+\frac{\beta-1}{f^4}}\left[S_{12}-\frac{1}{2}\frac{f^2-1}{f_{\max}^2-1}\sqrt{S_{11}+S_{22}} - \frac{a_2}{2}(f^2-1)\sqrt{|S_{11}-S_{22}|}\right]. \tag{1.178}$$

The enhanced slope of elongational viscosity of long-chain branched polymer melts in comparison to linear melts is caused by the fact that a significant percentage of the chain segments of a long-chain branched molecule is compressed by elongational flow (the *side chains*), and only part of the chain segments is stretched (the *backbone*). In the multi-chain segmental MSF model described here, for one chain segment stretched, $\beta-1$ chain segments are compressed. While for LDPE melts produced by the tubular polymerization processes typically values of $\beta=2$ are found, more highly branched autoclave LDPE melts show values of $\beta=3$ and even of $\beta=4$ (Fig. 1.16) [1.49].

The level of agreement between experiments in different extensional deformation modes and in start-up of steady shear flow and theory for a tubular LDPE melt with $\beta=2$ is demonstrated in Fig. 1.17 and Fig. 1.18.

Comparison of MSF Model Predictions to Elongational and Shear Rheology of Model Branched Polystyrene Melts. It is difficult if not impossible to derive the parameter β from the topology of randomly branched LDPE; therefore β in (see (1.175)) was treated as a fit parameter (the only one in the hyperelastic limit). However, from an analysis of the nonlinear rheology of comb shaped model polystyrene melts investigated by *Hep-*

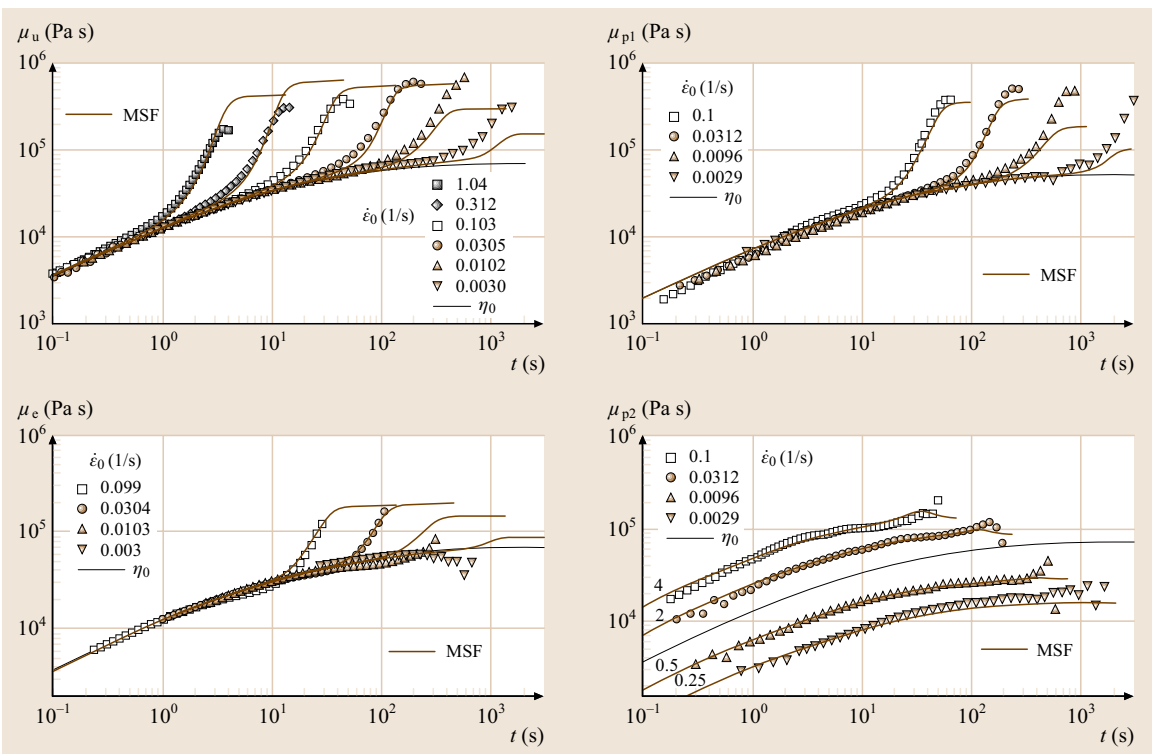

Fig. 1.17 Uniaxial (μ_u), equibiaxial (μ_e), and planar (μ_{p1}, μ_{p2}) viscosities of an LDPE melt. Viscosities are normalized with respect to the zero-shear viscosity. Comparison of experiment to predictions of the MSF model with dissipative constraint release. $f_{\max}^2=100$ (after [1.7])

perle and *Münstedt* [1.50, 56], it was found that indeed β, as derived from the topology of these model melts by assuming stretch of the backbone chain and compression of the side chains, is in quantitative agreement with experimental evidence seen in uniaxial extension [1.50]. The parameter β can simply be obtained as ratio of the number average molar mass of the grafted polymer, M_n, to the number average molar mass $M_{n,bb}$ of the backbone, which can be expressed in terms of the number average mass fraction $\Phi_{n,br}$ of grafted side chains,

$$\beta = \frac{M_n}{M_{n,bb}} = \frac{1}{1-\Phi_{n,br}} \,. \tag{1.179}$$

For linear polymers, naturally $\beta = 1$ is obtained from (1.179).

As exemplified in Fig. 1.19, agreement between predicted and observed slopes of the elongational viscosity after inception of strain hardening is excellent for all model branched polystyrene melts investigated. Within the experimentally accessible window of elongation rates, time–strain separability of the measured elongational viscosities is observed. Also, as far as a maximum strain-hardening could be determined, the data are compatible with the implicit assumption of the MSF model that the material parameter $f^2_{\max}$ is the same for all relaxation times of the terminal zone of the relaxation spectrum.

The shear damping function of model branched PS melts was measured by nonlinear shear relaxation experiments [1.50, 56]. Although the shear strain range investigated was limited to $\gamma < 5$, this is the impor-

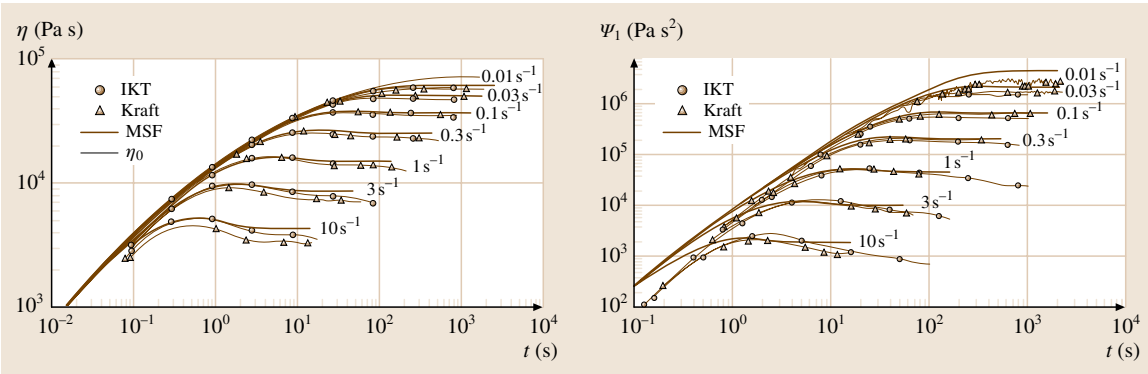

Fig. 1.18 Shear viscosity η and first normal stress function Ψ_1 of an LDPE melt. Comparison of experimental data (symbols) to predictions of the MSF model with dissipative constraint release $a_2 = 0.036$. For details see [1.7]

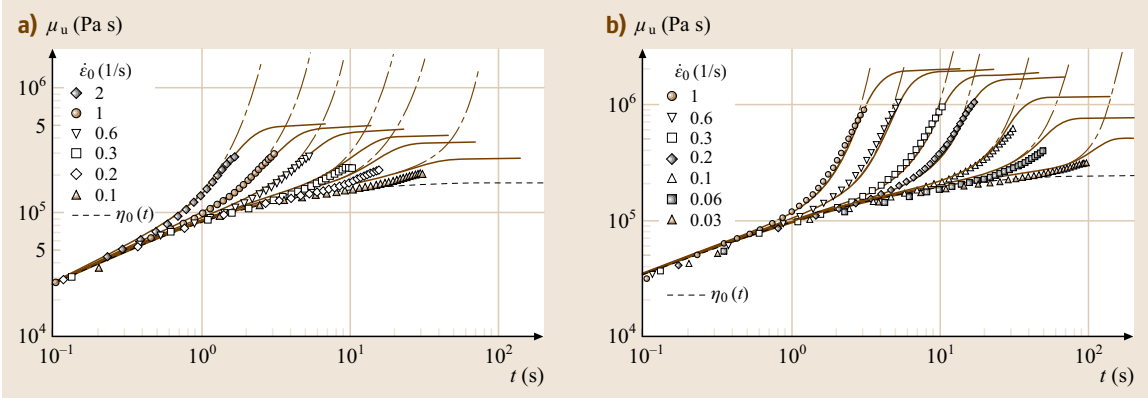

Fig. 1.19a,b Comparison of elongational viscosity data (*symbols*) of two branched PS melts to predictions (*lines*) of MSF theory. Viscosities are normalized with respect to the zero-shear viscosity; $\eta_0(t)$ indicates the start-up zero-shear viscosity [1.50, 56] . **(a)** PS 80-0.6G-22: $\Phi_{n,br} = 0.14$, $\beta = 1.2$; *dashed line*: $f^2_{\max} \to \infty$, *solid line*: $f^2_{\max} = 25$; **(b)** PS 70-3.2G-22: $\Phi_{\mathrm{n,br}} = 0.5$, $\beta = 2.0$; *dashed line*: $f^2_{\max} \to \infty$, *solid line*: $f^2_{\max} = 80$

tant shear strain range determining the shear stress in steady shear-rate flows. As is well known, branching also has significant influence on the shear strain behavior, although the effect is usually much smaller than in extensional flows [1.50, 56]: melts with high side-chain mass fractions show substantially less shear damping than melts with low side-chain mass fractions, and for shear strains up to 5, their shear damping functions are close to the hyperelastic or K-BKZ limit, i. e., the dissipative effect of constraint release is very small Fig. 1.20a. This agrees with earlier investigations of *Wagner* and *Ehrecke* [1.9] demonstrating that an LDPE melt shows reversible (or K-BKZ) behavior in double-step shear strain experiments in contrast to a (linear) polyisobutene melt, which showed *irreversible* behavior. With decreasing side chain mass fraction, the shear damping behavior of the model branched polystyrene melts approaches the behavior of linear polystyrene, and the influence of the parameter a_2 describing the additional dissipative constraint release due to rotational flow becomes important (Fig. 1.20b).

1.8.4 Conclusions

A survey of the most recent and most often used constitutive equations in nonlinear rheology shows the amount of progress made in the recent decades. It has shown that phenomenological constitutive integral equations can function as a rational basis of microstructural theories, but their relation to polymer structure remained elusive. Constitutive equations based on the tube model with pre-averaged chain stretch have been predominantly utilized by use of a differential approximation for the orientation tensors, and have been considered as appropriate for modeling of complex flows. The main problem of equations with pre-averaged chain stretch is the need to use a large number of nonlinear parameters, thereby losing any insight into the relation to polymer topology, and sometimes rendering the models too tedious even for a computer simulation.

Integral models with varying tube diameter have shown more flexibility in predicting polymer melt behavior in typical rheological flows, and have proven to be capable of describing the rheological behavior of a wide variety of polymers. The microstructural MSF model, which is based on the variable tube diameter idea, has been the latest among such constitutive equations with excellent predictive capabilities for modeling the nonlinear extensional and shear behavior of both linear and long-chain branched industrially important polymers. The concept of a strain-dependent tube diameter, which decreases with increasing deformation, explains consistently the strain hardening of linear as well as of long-chain branched polymer melts [1.7, 49, 50]. The steeper slope of the elongational viscosity after inception of strain hardening for branched melts in comparison to linear melts is due to the fact that in branched melts only a fraction (*the backbone*) of chain segments is stretched, while side chains are compressed [1.49, 50]. Long-chain branched polymer melts show reversible or *K-BKZ* behavior in double-step shear strain experiments, because dissipative constraint release occurs only at higher shear strains, in contrast to linear melts, where dissipation starts already at smaller shear strains [1.50].

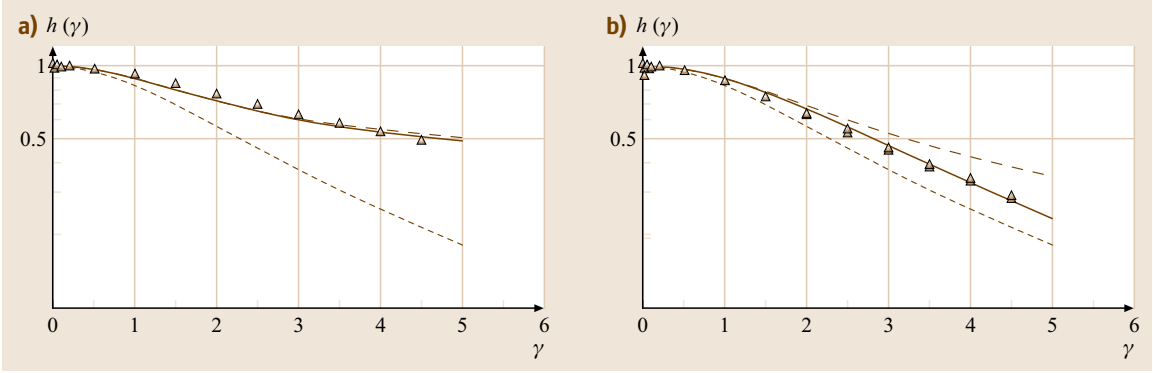

Fig. 1.20a,b Comparison of shear damping function data (*symbols*) of two PS melts to the predictions of the MSF theory [1.50, 56]; the *upper dash-dotted line* is the prediction assuming no constraint release (i. e., $f^2_{max} \to \infty$, $a_2 = 0$); the *lower dashed line* indicates the predictions of the Doi–Edwards IAA theory, i. e., $f^2_{max} \equiv 1$ [1.50]. **(a)** Branched PS 70-3.2G-22: the *full line* is the prediction of the MSF model with the parameters $\beta = 2$, $f^2_{max} = 80$ and $a_2 = 0$; **(b)** linear PS-r-95: the *full line* is the prediction of the MSF model with the parameters $\beta = 1$, $f^2_{max} = 6$ and $a_2 = 0.4$

Challenges in nonlinear rheology remaining are, to mention just a few, the relations between macromolecular architecture of homopolymers and the nonlinear parameters f_{max}^2 and a_2 of the MSF theory, as well as modeling the nonlinear rheology of blends of linear and long-chain branched polymers.

References

1.1 S.I. Green: *Fluid Vorticies* (Kluwer Academic, Dordrecht 1995)

1.2 D.D. Joseph: *Fluid Dynamics of Viscoelastic Liquids* (Springer, Berlin 1990)

1.3 R.G. Larson: *Constitutive Equations for Polymer Melts and Solutions* (Butterworths, London 1988)

1.4 M. Doi, S.F. Edwards: *The Theory of Polymer Dynamics* (Oxford Univ. Press, Oxford 1986)

1.5 M.H. Wagner: *Challenges in Nonlinear Rheology of Linear and Long-Chain Branched Polymer Melts* (Proc. XIVth Int. Congr. On Rheology, Korea 2004)

1.6 T.C.B. McLeish, S.T. Milner: Entangled dynamics and melt flow behavior of branched polymers, Adv. Polym. Sci. **143**, 195–256 (1999)

1.7 M.H. Wagner, P. Rubio, H. Bastian: The molecular stress function model for polydisperse and polymer melts with dissipative convective constraint release, J. Rheol. **45**, 1387–1412 (2001)

1.8 H. Bastian: *Non-linear viscoelasticity of linear and long-chain-branched polymer melts in shear and extensional flows , Ph. D. Thesis* (Universität Stuttgart, Stuttgart 2000), http://elib.uni-stuttgart.de/opus/volltexte/2001/894

1.9 M.H. Wagner, P. Ehrecke: Dynamics of polymer melts in reversing shear flows, J. Non-Newtonian Fluid Mech. **76**, 183–197 (1998)

1.10 A.S. Lodge: Constitutive equations from molecular theories for polymer solutions, Rheol. Acta. **7**, 379–392 (1968)

1.11 E. van Ruymbeke, R. Keunings, V. Stéphenne, A. Hagenaars, C. Bailly: Evaluation of reptation models for predicting the linear viscoelastic properties of linear entangled polymers, Macromolecules **35**, 2689–2699 (2002)

1.12 A.L. Frischknecht, S.T. Milner, A. Pryke, R.N. Young, R. Hawkins, T.C.B. McLeish: Rheology of three-arm asymmetric star polymer melts, Macromolecules **35**, 4801–4820 (2002)

1.13 M.H. Wagner, J. Meissner: Network disentanglement and time-dependent flow behavior of polymer melts, Macromol. Chem. **181**, 1533–1550 (1980)

1.14 C.W. Macosko: *Rheology, Principles, Measurements and Applications* (VCH, New York 1994)

1.15 H.M. Laun: Description of the non-linear shear behavior of a low density polyethylene melt by means of an experimentally determined strain dependent memory function, Rheol. Acta. **17**, 1–15 (1978)

1.16 M.H. Wagner: Analysis of time-dependent non-linear stress-growth data for shear and elongational flow of a low-density branched polyethylene melt, Rheol. Acta. **15**, 136–142 (1976)

1.17 M.H. Wagner: Prediction of primary normal stress difference from shear viscosity data using a single integral constitutive equation, Rheol. Acta. **16**, 43–50 (1977)

1.18 M.H. Wagner, S.E. Stephenson: The spike strain test for polymeric liquid and its relevance for irreversible destruction of network connectivity by deformation, Rheol. Acta. **18**, 463–468 (1979)

1.19 M.H. Wagner, S.E. Stephenson: The irreversibility assumption of network disentanglement in flowing polymer melts and its effects on elastic recoil predictions, J. Rheol. **23**, 489–504 (1979)

1.20 K. Osaki, S. Kimura, M. Kurata: Relaxation of shear and normal stresses in double-step shear deformations for a polystyrene solution. A test of Doi-Edwards theory for polymer rheology, J. Rheol. **25**, 549–562 (1981)

1.21 M.H. Wagner: A constitutive analysis of uniaxial elongational flow data of a low-density polyethylene melt, J. Non-Newtonian Fluid Mech. **4**, 39–55 (1978)

1.22 A.C. Papanastasiou, L.E. Scriven, C.W. Macosko: An integral constitutive equation for mixed flows: viscoelastic characterization, J. Rheol. **27**, 387–410 (1983)

1.23 T. Samurkas, R.G. Larson, J.M. Dealy: Strong extensional and shearing flows of a branched polyethylene, J. Rheol. **33**, 559–578 (1989)

1.24 P.K. Currie: Constitutive equations for polymer melts predicted by the Doi–Edwards and Curtiss-Bird kinetic theory models, J. Non-Newtonian Fluid Mech. **11**, 53–68 (1982)

1.25 M.H. Wagner, A. Demarmels: A constitutive analysis of extensional flows of polyisobutylene, J. Rheol. **34**, 943–958 (1990)

1.26 O. Urakawa, M. Takahashi, T. Masuda, N.G. Ebrahimi: Damping functions and chain relaxation in uniaxial and biaxial elongation: comparison with the Doi-Edwards theory, Macromolecules **28**, 7196–7201 (1995)

1.27 B.J.R. Scholtens, P.J.R. Leblans: Nonlinear viscoelasticity of noncrystalline EPDM rubber networks, J. Rheol. **30**, 313–335 (1986)

1.28 M.H. Wagner: The nonlinear strain measure of polyisobutylene melt in general biaxial flow and its comparison to the Doi-Edwards model, Rheol. Acta. **29**, 594–603 (1990)

1.29 D.S. Pearson, A. Kiss, L. Fetters, M. Doi: Flow-induced birefringence of concentrated polyisoprene solutions, J. Rheol. **33**, 517–535 (1989)

1.30 G. Ianniruberto, G. Marrucci: A simple constitutive equation for entangled polymers with chain stretch, J. Rheol. **45**, 1305–1318 (2001)

1.31 J. Fang, M. Kröger, H.M. Öttinger: A thermodynamically admissible reptation model for fast flows of entangled polymers: II. Model predictions for shear and extensional flows, J. Rheol. **44**, 1293–1316 (2000)

1.32 T.C.B. McLeish, R.G. Larson: Molecular constitutive equations for a class of branched polymers: the pom-pom polymer, J. Rheol. **42**, 81–110 (1998)

1.33 T.C.B. McLeish: Molecular rheology of H-polymers, Macromolecules **21**, 1062–1070 (1988)

1.34 N.J. Inkson, T.C.B. McLeish, O.G. Harlen, D.J. Groves: Predicting low density polyethylene melt rheology in elongational and shear flows with pom-pom constitutive equations, J. Rheol. **43**, 873–896 (1999)

1.35 R.J. Blackwell, T.C.B. McLeish, O.G. Harlen: Molecular drag-strain coupling in branched polymer melts, J. Rheol. **44**, 121–136 (2000)

1.36 R.G. Owens, T.N. Phillips: *Computational Rheology* (Imperial College Press, London 2002)

1.37 P. Rubio, M.H. Wagner: Letter to the Editor: A note added to "Molecular constitutive equations for a class of branched polymers: The pom-pom model", J. Rheol. **43**, 1709–1710 (1999)

1.38 P. Rubio, M.H. Wagner: LDPE melt rheology and the pom-pom polymer, J. Non-Newtonian Fluid Mech. **92**, 245–259 (2000)

1.39 R.J. Blackwell, O.G. Harlen, T.C.B. McLeish: Theoretical linear and non-linear rheology of symmetric treelike polymer melts, Macromolecules **34**, 2579–2596 (2001)

1.40 P.J. Doerpinghaus, D.G. Baird: Accessing the branching architecture of sparsely branched metallocene-catalyzed polyethylenes using the pompom constitutive model, Macromolecules **35**, 10087–10095 (2002)

1.41 W.M.H. Verbeeten, G.W.M. Peters, F.P.T. Baaijens: Differential constitutive equations for polymer melts: The extended pom-pom model, J. Rheol. **45**, 823–843 (2001)

1.42 N. Clemeur, R.P.G. Rutgers, B. Debbaut: On the evaluation of some differential formulations for the pom-pom constitutive model, Rheol. Acta. **42**, 217–231 (2003)

1.43 G. Marrucci, B. de Cindio: The stress relaxation of molten PMMA at large deformations and its theoretical interpretation, Rheol. Acta. **19**, 68–75 (1980)

1.44 M.H. Wagner, J. Schaeffer: Constitutive equations from Gaussian slip-link network theories in polymer melt rheology, Rheol. Acta. **31**, 22–31 (1992)

1.45 M.H. Wagner, J. Schaeffer: Rubbers and Polymer melts: Universal aspects of non-linear stress-strain relations, J. Rheol. **37**, 643–661 (1993)

1.46 M.H. Wagner: The non-linear strain measure of polymer melts and rubbers: A unifying approach, Makromol. Chem. Macromol. Symp. **68**, 95–108 (1993)

1.47 M.H. Wagner, J. Schaeffer: Assessment of non-linear strain measures for extensional and shearing flows of polymer melts, Rheol. Acta. **33**, 506–516 (1994)

1.48 M.H. Wagner, J. Schaeffer: Nonlinear strain measures for general biaxial extension of polymer melts, Rheol. Acta. **36**, 1–26 (1992)

1.49 M.H. Wagner, M. Yamaguchi, M. Takahashi: Quantitative assessment of strain hardening of LDPE melts by MSF model, J. Rheol. **47**, 779–793 (2003)

1.50 M.H. Wagner, J. Hepperle, H. Münstedt: Relating molecular structure of model branched polystyrene melts to strain-hardening by molecular stress function theory, J. Rheol. **48**, 489–503 (2004)

1.51 M.H. Wagner, S. Kheirandish, M. Yamaguchi: Quantitative analysis of melt elongational behavior of LDPE/LLDPE blends, Rheol. Acta **44**, 198–218 (2005)

1.52 M.H. Wagner, S. Kheirandish, K. Koyama, A. Nishioka, A. Minegishi, T. Takahashi: Modeling strain hardening of polydisperse polystyrene melts by molecular stress function theory **44**, 235–243 (2005)

1.53 P.G. de Gennes: Reptation of polymer chain in the presence of fixed obstacles, J. Chem. Phys. **55**, 572–579 (1971)

1.54 G. Marrucci, N. Grizzutti: The free energy function of the Doi-Edwards theory: Analysis of instabilities in stress relaxation, J. Rheol. **27**, 433–450 (1983)

1.55 G. Marrucci, J.J. Hermans: Non-linear viscoelasticity of concentrated polymeric liquids, Macromolecules **13**, 380–387 (1980)

1.56 J. Hepperle: *Einfluss der molekularen Struktur auf rheologische Eigenschaften von Polystyrol- und Polycarbonatschmelzen* (Shaker, Aachen 2003)